Sensitivity of tropospheric loads and lifetimes of short lived pollutants to fire emissions

N. Daskalakis[1,2], S. Myriokefalitakis[1], and M. Kanakidou[1]

[1]((Environmental Chemical Processes Laboratory, Department of Chemistry, University of Crete, Heraklion, Crete, Greece))

[2]((Institute of Chemical Engineering Sciences (ICE-HT), FORTH, Patra, Greece))

Correspondence to: M. Kanakidou (mariak@chemistry.uoc.gr)

Abstract

The capability of global Chemistry and Transport Models (CTMs) to simulate atmospheric composition and its spatial and temporal changes highly relies on the input data used by the models, in particular the emission inventories. Biomass burning emissions show large spatial, diurnal, seasonal and year-to-year variability. In the present study, we applied a global 3D CTM to evaluate uncertainties in the computed atmospheric composition associated with the use of different biomass burning emissions and identify areas where observational data can help to reduce these uncertainties. We find the emission inventory choice to lead to regional differences in the calculated load of aerosols up to a factor of 4. Assumptions on the injection height of the biomass burning emissions are found to produce regionally up to 30% differences in the calculated tropospheric lifetimes of pollutants. Computed changes in lifetimes point to a strong chemical feedback mechanism between emissions from biomass burning and isoprene emissions from vegetation that are linked via NO_x-driven oxidant chemistry, NO_x-dependent changes in isoprene oxidation products, aerosol emissions and atmospheric transport. These interactions reduce isoprene load in the presence of biomass burning emissions by 15%, calculated for the same amount of isoprene emitted into the troposphere. Thus, isoprene load and lifetime are inversely related to the quantities of pollutants emitted by biomass burning. This feedback is shown to be able to increase the apparent secondary aerosol yield from isoprene, defined as the ratio of tropospheric loads of secondary aerosol from isoprene oxidation to that of isoprene, by up to 40%.

1 Introduction

Atmospheric composition is affected by emissions of reactive gases and aerosols to the atmosphere by several natural (e.g. soils, vegetation, oceans, volcanoes, wild fires) and anthropogenic sources (e.g. industrial and residential activities, transport, and shipping). Among these sources biomass burning plays a central role for atmospheric chemistry via changes in the atmospheric composition but also impacting on the ecosystem functioning through atmospheric deposition of nutrients and the lifecycle of vegetation (Keywood et al., 2013). Biomass burning is positioned between the natural (wild fires) and human-induced (intentional burning) sources of atmospheric pollutants since a fraction of open fires is induced by humans for agricultural and city expansion purposes (Levine et al., 1995) or for protection against fire itself (Mutch, 1994). Biomass burning is an important source of trace constituents to the atmosphere including radiatively and chemically reactive gases and aerosols (Akagi et al., 2011; Andreae and Merlet, 2001). It is the largest source of primary carbonaceous aerosols (Bond et al., 2004) and the second largest source of volatile organic compounds (VOC) in the atmosphere after the emissions from vegetation (Guenther et al., 2012) and of carbon monoxide (CO) after anthropogenic emissions (Kanakidou and Crutzen, 1999; Pfister et al., 2005).

Emissions from biomass burning and their transformation in the atmosphere affect air quality (Lelieveld et al., 2004), interact with radiation (Reid et al., 2005) and the atmospheric water cycle and thus affect climate (Rosenfeld, 1999). In turn climate change is seen to impact on wild fire occurrence and intensity. For instance the exceptionally intensive 1997/1998 Indonesia fires have been attributed to the combined strength of the El Niño and the Indian Ocean Dipole (Field et al., 2009).

Significant changes in the trends of atmospheric concentrations of CH_4 and CO have been attributed to the changes in the biomass burning emissions (Simmonds et al., 2005). Most of these emissions occur in the tropics that are subject to intensive photochemistry in the presence of high humidity conditions and significant convective activities (Chatfield and Delany, 1990; Crutzen, 1994). During summer in the high latitudes boreal forest fires contribute about 12% to the global biomass burning emissions (Lavoué et al., 2000) and can be so intensive and convective that their emissions reach the high troposphere and low stratosphere (Fromm et al., 2000).

Tropical photochemistry is controlling the lifetime of most atmospheric pollutants (Crutzen, 1994; Keywood et al., 2013), including reactive greenhouse gases like methane (CH_4) and ozone (O_3), and thus their persistence in the atmosphere to impact on radiation and climate. Up to about 25% of the net global photochemical production of tropospheric ozone has been attributed to biomass burning emissions and chemistry in the atmosphere (Crutzen and Andreae, 1990; Jaffe and Wigder, 2012). Long range transport of biomass burning aerosols has been seen to happen fast within one or two weeks both downwind tropical (Dirksen et al., 2009; Edwards et al., 2006) and high latitude sources (Jaffe et al., 2004). Thus this source is affecting atmospheric pollutant levels in remote environments. For instance, chemical ageing of fire plumes has been identified as contributor to the high ozone over the Atlantic ocean (Lelieveld et al., 2004). Therefore it is important to simulate the impact of biomass burning emissions on tropospheric composition and pollutant lifetimes and to evaluate the uncertainties in such simulations.

Several biomass burning emission inventories have been constructed based on burned area, active fire detections, and plant productivity from satellite observations (van der Werf et al., 2010) or on assimilated Fire Radiative Power derived from satellite observations (Kaiser et al., 2012) and experimentally determined pollutant emission factors (Andreae and Merlet, 2001) and assumptions on the state of burning of the biomass (smoldering or flaming, van der Werf et al. (2006)). All these factors introduce uncertainties in the emissions (Granier et al., 2011; Wiedinmyer et al., 2011). In particular, the size of small fires can be overestimated and the number of fires can be underestimated when seen by satellites (Wiedinmyer et al., 2011). The injection height of fire emissions (Dentener et al., 2006; Freitas et al., 2007; Sofiev et al., 2012) is an additional cause of discrepancies in the model estimates of the impact of these fires on tropospheric composition. The height distribution proposed by Dentener et al. (2006) (used in this work) is based on wildfire location and type, where the distribution described in Sofiev et al. (2012) is based on the fire characteristics (fire intensity, temperature of plume, type of source) as well as the meteorological conditions (atmospheric boundary layer height, free troposphere). These two approaches show similarities in emission heights over North America and Oceania, but over Eurasia, Australia and South America the two methods show significant differences (Sofiev et al., 2013). A plume height climatology over North America has been also derived by analysis of 5-year satellite observations by MISR (Val Martin et al., 2010) which compared to the Dentener et al (2006) vertical distribution of fires there (2000-

6000 meters) shows lower mean injection heights (500-1500 meters) for boreal fires but is in agreement for temperate and tropical fires. Plume rise models evaluated against that climatology have been shown to underestimate the observed plume heights (Val Martin et al., 2012). Guan et al. (2008) using the NCAR CAM3.1 model found that the calculated CO concentrations downwind biomass burning emission areas, can increase by up to 150 ppb depending on the assumptions in the injection height of the emissions. Boreal forest fire emissions occurring high in the troposphere have been detected by Colarco et al. (2004) to be transported from Canada to Washington D.C. in the U.S.A. where they have been mixed with boundary layer air. Long range transport of biomass burning pollutants has been followed by lidar and satellite observations and the simulations have been shown to be sensitive to the injection height of the emissions as well as to the entrainment of air into the boundary layer over U.S.A. Note that boreal fires plumes can reach the upper troposphere where their impact is different from that in the boundary layer due to the non-linearities in the atmospheric chemistry (Chatfield and Delany, 1990) and the different photochemical conditions there. Leung et al. (2007) global modeling study of the impact of boreal fire emissions on air pollutants levels, found a much larger enhancement in ozone when about half the emissions were released above the boundary layer than when all emissions were occurring in the boundary layer. They attributed these differences to the role of peroxyacetyl nitrate (PAN) as carrier of NO_x downwind burning areas. Jaffe et al. (2004) found that the intensive Siberian fires in 2003 enhanced the background ozone over the Pacific Norhwest U.S.A., resulting to exceedance of ozone air quality standard. Hodzic et al. (2006) studying AOT over Europe during the 2003 Portuguese fires identified high altitude transport of smoke particles from Portugal to The Netherlands, that has been both observed by POLDER-2 and simulated by the CHIMERE model. Williams et al. (2012) simulated the African fires in 2005 using the TM4 model and three different biomass burning emission inventories, two global and one regional. They calculated differences in the ozone global burden resulting from the use of different biomass burning inventories that range between +1.7% and +4.6% compared to the simulation using GFEDv3 biomass burning emission inventory.

The present study aims to evaluate uncertainties in model estimates of biomass burning impacts on atmospheric composition that are associated with the use of different emission inventories in the same model. The study also aims to identify locations where additional observations can provide constrains for biomass burning emission estimates. For this purpose

a global 3D Chemistry and Transport Model (CTM) is applied to evaluate uncertainties in the atmospheric composition and major pollutants lifetimes computed using recently updated and commonly used biomass burning emissions. Based on the computed model sensitivity to biomass burning emissions, we also identify areas where observational data can help to reduce these uncertainties.

2 Model Description

The model used for this study is the global 3-D CTM TM4-ECPL (Kanakidou et al., 2012). The model accounts for gas and multiphase chemistry to describe tropospheric ozone chemistry and all major aerosol components (primary and secondary). It contains explicit chemistry of C_1 to C_5 volatile organic compounds (VOCs) and a highly simplified representation of *a*-pinene and *β*-pinene chemistry. The model calculates secondary organic aerosol (SOA) formation by VOC oxidation and subsequent gas-to-particle partitioning of semivolatile products (Tsigaridis and Kanakidou (2007) as updated by Myriokefalitakis et al. (2010)). Chemical aging of organic aerosol (OA) is also taken into account. For primary organic aerosol (POA) and black carbon (BC) chemical ageing is considered to occur by oxidation of organic material that coats the particles and is driven by O_3 (Tsigaridis and Kanakidou, 2003); while for SOA chemical ageing to non-volatile SOA (Tsigaridis and Kanakidou, 2003) is considered to occur by reaction with OH at the rate of 4.10^{-12} molec^{-1}cm^{3}s^{-1}, very close to that of the H-abstraction reaction of pinonic acid with OH (Praplan et al., 2012). BC emissions are by 20% soluble while terrestrial POA emissions are by 50% soluble. For both BC and POA the insoluble fraction is converted to soluble during aging. Multiphase chemical production of SOA is parameterized as described in Myriokefalitakis et al. (2011). Gas-to-particle partitioning of inorganic components is solved using the ISORROPIA II aerosol thermodynamic model that also calculates the aerosol-water (Fountoukis and Nenes, 2007; Nenes et al., 1998). For this study the TM4-ECPL model uses a 3°x2° longitude-latitude grid and 34 hybrid levels up to 0.1 hPa (with the first 4 model vertical layers between surface and 900 hPa) and is driven by the European Centre for Medium-range Weather Forecasts (ECMWF) ERA-Interim meteorological data (Dee et al., 2011) for the year 2008 for all the sensitivity simulations.

2.1 Natural emissions

Isoprene, terpenes and biogenic volatile organic compounds (BVOC) emissions in the TM4-ECPL model are taken from the MEGAN-MACC inventory (Sindelarova et al., 2014) for the year 2008, which is a product of the MEGANv2.1 model (Guenther et al., 2012). Dust emissions are from AeroCom (Aerosol Comparisons between Observations and Models; (Dentener et al., 2006) calculated for the year 2008 by E. Vignati (personal communication, 2011). Marine emissions of sea-salt aerosols and organic gases and aerosols are calculated online driven by meteorology and sea water productivity as described by Myriokefalitakis et al. (2010) and Vignati et al. (2010).

2.2 Anthropogenic emissions

Anthropogenic emissions used for this experiment are the ECLIPSE (Evaluating the CLimate and Air Quality ImPacts of Short-livEd Pollutants) version 4.0 emissions (Klimont et al., 2013), available in 0.5°x0.5° spatial resolution. The ECLIPSE anthropogenic inventory was initially provided as sectoral including the agricultural waste burning sector (AWB). Since AWB is either included in the anthropogenic emissions or in the biomass burning emissions, caution was taken to avoid double counting of the emissions. For this, the AWB emissions (Table 3) are considered separately for the simulations that have been performed for this study (Table 4). The AWB in the ECLIPSE database amounts to 4.5% of the total anthropogenic pollutants emissions (approximately 34.5 Tg a^{-1}) for the year 2008 (see Table 1 for more information). Anthropogenic emissions of all basic pollutants are used (CO, nitrogen oxides (NO_x), black carbon aerosol (BC), particulate organic carbon (OC), sulfur dioxide and sulfates (SO_x) as well as speciated non methane volatile organic compounds (NMVOCs; for a list of the NMVOCs used in the model see supplementary material S1).

2.3 Biomass burning emissions

For the present study a number of sensitivity simulations have been performed (Table 4) using different biomass burning emissions (Table 2) and AWB emissions (Table 3), all for the year 2008. For the base simulation (S0.0), the biomass burning emissions from the Global Fire Emission Database v 3.1 (GFEDv3; van der Werf et al. (2010)) are used, excluding the AWB sector (Table 3), hereafter called GFEDv3-ECLIPSE biomass burning emissions (S0.X), while AWB emissions are taken from the ECLIPSE anthropogenic emissions developed in the

framework of the ECLIPSE project. Additional simulations have been performed (Table 4) using both biomass burning and AWB emissions from the GFEDv3 (van der Werf et al., 2010) (S1.X), as well as AWB from ECLIPSE and biomass burning emissions from the Atmospheric Chemistry and Climate Model Intercomparison Project's (ACCMIP; Lamarque et al. (2013); http://ecaad.sedoo.fr) (S2.X) or from the Fire INventory from NCAR (FINN; Wiedinmyer et al. (2011) http://bai.acd.ucar.edu/Data/fire/) (S3.X) and finally a simulation where no biomass burning emissions were taken into account (S4.0). Since the injection height of these emissions contributes to the uncertainty of the model results, biomass burning emissions are considered in the model either to be injected at heights following Dentener et al. (2006), or to be emitted solely in the lowest model layer (see list of simulations in Table 4). The temporal variability of theses biomass burning inventories per emitted species for 2008 is shown in Fig. 1. This figure depicts the differences between the inventories in their seasonality and amplitude (also annual totals in Table 2); while Fig S2 in the supplementary material shows spatial difference in the annual BC emissions between the inventories. The ACCMIP inventory shows the largest magnitude in the temporal variation of these emissions. All inventories show a July-Sept. primary maximum while they differ in the secondary maximum between Jan and April. The AWB emissions that are not included in the GFEDv3-ECLIPSE biomass burning inventory significantly contribute to NMVOC and NH_3 emissions during spring and summer.

3 Experiment setup

The impact of the use of different biomass burning emission inventories to the calculated tropospheric loads and lifetimes of the main pollutants and the sensitivity of the model results to the wild fire emissions have been evaluated based on nine different simulations. For all simulations the model setup was exactly the same, except for the biomass burning emissions inventory used and its vertical distribution application. A summary of the simulations here performed is provided in Table 4. The GFEDv3-ECLIPSE inventory and height distribution for biomass burning emissions have been used as the base case scenario (S0.0). All scenarios named SX.0 assume the same fractional height distribution of the emissions according to Dentener et al. (2006) where all the scenarios named SX.1 assume all open biomass burning emissions to occur at surface. For scenario S4.0, open biomass burning emissions are set to zero. Note that we have chosen to account for monthly mean emissions since not all

inventories have higher temporal resolution. This is the reason we have also chosen to validate the model results comparing to monthly mean observations.

4 Results

To evaluate the ability of the model to reproduce the observations, the computed concentrations are compared with measurements. The differences in the fields computed by the various emission inventories provide a measure for the robustness of the model results with regard to the biomass burning impacts. Comparison of the simulated tropospheric concentrations of pollutants between the various scenarios reveals the spatial and temporal differences due to the different inventories and could indicate which inventory is performing the best. Ultimately these differences will point to areas where additional observations can contribute to reduce uncertainties of the emission inventories as will be further discussed. Finally, tropospheric lifetimes are calculated to provide information on how the location and strength of the emissions affect the persistence of the pollutants in the atmosphere.

4.1 Comparison with ground measurements

Surface observations of Ozone from the European Monitoring and Evaluation Programme (EMEP) monitoring network (Europe), Ozone and CO observations from the World Data Centre for Greenhouse Gases (WDCGG) database (Global) and particulate Organic Carbon (OC) observations from the Aerosol Comparisons between Observations and Models (AeroCom) phase II database (Global) (Tsigaridis et al., 2014) have been used for the model evaluation. The locations of measurements are shown in Fig. S1 in the supplement. While all available data have been used for model evaluation, only comparisons at stations that have been selected to make evident differences between the simulations using different biomass burning emission inventories are shown for OC (Fig. 2), CO (Fig. 3) and O_3 (Fig. 4). Concentration fields of primary pollutants emitted by biomass burning are more strongly affected by the different emission inventories and injection heights. Thus, OC computed concentrations (Fig. 2) and BC concentrations (not shown) present the largest diversity, between simulations followed by CO (Fig. 3), which is emitted by fires, but has also secondary sources.

The simulated OC for the various scenarios and their differences from the observations in the tropics, the subtropics and high latitudes at locations affected by biomass burning emissions

are shown in Fig. 2. Due to limited observational data from the tropics where most of the biomass burning occurs, for the following comparisons all available data have been used independent of the year. Modeled differences for OC due to emission inventory choice can exceed a factor of three at Alta Floresta (Fig. 2c) and eight at Rondonia (Fig. 2d) during the biomass burning months. Using the ACCMIP inventory the largest OC levels are computed at the tropical station of Alta Floresta in August and September, whereas the GFEDv3-ECLIPSE and GFEDv3 inventories include large amounts of OC injections at the subtropical stations of California in June, July and August (Fig. 2b and g). Different emission inventories significantly affect the model performance over and downwind locations where wildfires occur. Unfortunately, current observational sites do not provide sufficient constraint for the emission databases evaluation.

Tsigaridis et al. (2014) OC global model intercomparison exercise has indicated that among the thirty-one models contributing to that study, some models emit all biomass burning aerosols at the surface, while most models distribute them to a number of layers above the surface, typically within the boundary layer. Most models are using GFEDv3 and ACCMIP inventories and all models appear to have similar seasonality in primary OC emissions with increased emissions during Northern Hemisphere summer due to the enhanced contribution of Northern Hemisphere biomass burning emissions from temperate and boreal forests to the total OC fluxes. Kaiser et al. (2012) found systematic model underestimation of smoke aerosol optical depth (AOD) observed by MODIS that can be as high as a factor of 3 on the global scale when emissions from bottom-up inventories like GFED are used. Petrenko et al. (2012) have demonstrated that such underestimate strongly varies by region.

Similar to OC results are obtained for CO, as seen in Fig. 3, where during the biomass burning season different quantities of CO are calculated depending on the inventory used. At Yonagunijima (Fig. 3a) CO concentration differences computed using the different inventories maximize in spring and models are underestimating measurements by 25%. Such differences between inventories are large at the East Trout Lake station in Canada, where in June and July model results differ by up to 150 ppb (a factor of 2.5). These results reflect the extremely high emissions in the GFEDv3-ECLIPSE and GFEDv3 inventories for this region that are not seen in the measurements (Fig. 3b). The assumption that all emissions occur near the surface leads to about 60% higher CO surface concentrations than when emissions are distributed vertically. At the areas where biomass burning occurs and downwind of them,

these emissions contribute between 10 and 75% to the total CO levels during the burning season.

Comparisons of O_3 simulations with surface measurements (Fig. 4) show noticeable difference between the simulation that neglects wildfire emissions (S4.0) and all other simulations, at stations like Mt. Kenya (Fig. 4f), La Quiaca observatory (Fig. 4g) and Hok Tsui (Fig. 4d), which are located in the vicinity or outflow of tropical biomass burning. These are areas where O_3 levels are the most sensitive to the different biomass burning emission scenarios. For instance, at La Quiana observatory (Fig. 4g), differences as high as 10 ppb of O_3 (i.e. ~25%) are computed for October when using the different emission scenarios. The FINN inventory results in the highest computed O_3 levels, while omitting biomass burning reduces O_3 levels by ~35%. However, very small sensitivity is seen between the scenarios with wildfire emissions for the other locations in Fig. 4. Thus, evaluating these inventories requires densifying air quality monitoring close to the major biomass burning sources in the tropics, which are virtually absent. Furthermore, we have calculated the ratio of the standard deviation to the mean of all model simulations to identify locations where biomass burning emission inventories produce the largest model divergence. In Fig. 5 these ratios are shown for OC and indicate that systematic observations over boreal regions, Alaska, South Asia and Indonesia can help constrain the used biomass burning emission inventories.

4.2 Comparison with ozonesondes and satellite observations

Because the impact of biomass burning is not restricted to the surface concentrations of pollutants but also extends in the free troposphere, we have also compared model results with ozonsondes as well as with O_3 and CO mid tropospheric columns as observed by Tropospheric Emission Spectrometer (TES) satellite instrument. In addition, simulated O_3 profiles have been compared with available ozonesondes data from WDCGG after interpolating into layers of 50 hPa from surface to the top of the atmosphere as described in detail by Myriokefalikakis et al. (2015 in preparation). Figure S6 in the supplement shows that there is no statistical difference in the performance of the different scenarios with regard to ozonesonde observations.

Similar results are obtained from the comparison of model results to the TES global survey data version 4 with focus on the relatively sensitive in the middle/lower free troposphere, using data from 7 TES pressure levels between 800 and 400 hPa. The TES products are

provided in 67 levels in vertical with a varying layer thickness (Beer et al., 2001). In order to compare TM4-ECPL model results with the TES observations, the methods presented in (Voulgarakis et al., 2011) have been used. Thus, the 3 – hourly model outputs are sampled at the times and locations of the TES measurements, then they are interpolate onto the 67 TES pressure levels in vertical, and finally the TES a priori profiles and averaging kernels are applied. The processed observational and model data are regridded to original 3^ox2^o in longitude by latitude horizontal resolution in order to smooth – out gaps in the observations. More details are provided in Myriokefalitakis et al. (in preparation, 2015) where a detailed model evaluation is presented including comparison with satellite observations.

Point-by-point comparisons of the results for the different simulations performed for the present study against available TES observations for all model grids on daily mean basis are shown in Figures S7 in the supplement. No simulation and thus no emission database stands out for its performance in reproducing the observations.

4.3 Tropospheric loads

The global annual mean tropospheric loads for selected gases and aerosol components as computed for the base case scenario (S0.0) are shown in Fig. 6 for OC, CO, NOx, O_3, OH, and isoprene. Fig. S3 (in the supplement) shows similar results for BC, SO_4^{2-}, NO_3^-, HNO_3 and NH_4^+. Although changes in the wildfire emissions do not significantly impact the global tropospheric load of most pollutants as shown in Table 5, regionally significant differences are computed (e.g. for BC, the difference can reach a factor of 7, Fig. S4b) as will be further discussed. The choice of wildfire emission inventory impacts on the calculated tropospheric load of tracers. The most sensitive pollutants to wildfire emissions are found to be OC and BC, while O_3 shows small sensitivity.

4.3.1 Contribution of wildfires emissions on tropospheric loads.

The contribution of wildfires to the tropospheric load of pollutants can be calculated by comparison of S0.0 (base case) with S4.0 that neglects the emissions. Wildfires increase the tropospheric loads of: OC by ~30%, BC by ~35%, CO by about 13% , NH_4^+ by 10%, HNO_3 by 8%, NO_x by 5%, and SO_4^{2-} and O_3 by 3% (Table 5).

Previous studies for CO with the NOAA GFDL GCTM have shown biomass burning to contribute from 15 to 30% to the total CO background (Galanter et al., 2000). This is in

agreement with the measurements by Crounse et al. (2009) in central Mexico which attributed 21-31% of CO load to biomass burning emissions. This impact presents large temporal and spatial variability since it occurs during the burning season that lasts only a few months per year and is marked by tropical and boreal forest fires. Ziemke et al. (2009) modeling study with the Global Modeling Initiative (GMI) chemical transport model shows a global increase in CO between 21% and 53% due to biomass burning. The tropospheric O_3 load has been shown to correlate with that of CO during biomass burning events with a slope of O_3/CO of about 1 (Honrath et al., 2004). However, other studies have shown only small changes in the tropospheric ozone on global scale (4-5% increase computed by Ziemke et al. (2009)), where regionally different impacts are computed, ranging for 10%-40% increase depending on region and season (Galanter et al., 2000). Aircraft observations in Boreal Canada showed no distinguishable within the smoke plume and in clean air (Parrington et al., 2013), while substantial O_3 enhancement has been measured in air masses downwind fire locations (Palmer et al., 2013).

The spatial variability of the annual mean impact of wildfire emissions on the tropospheric loads of OC, CO, NO_x, O_3, OH and isoprene is depicted in Fig. 7a-f and on BC, SO_4^{2-}, NO_3^-, HNO_3 and NH_4^+ in Fig. S5a-e (supplement). The most affected pollutants are OC (Fig. 7a) and BC (Fig. S5a) with computed local reduction due to the omission of wildfires by almost 100%, in agreement with previous studies where a reduction of 50 % has been measured in Beijing (Duan et al., 2004), and up to 66% in Central Mexico (Crounse et al., 2009). Our results also show that annual mean local impacts on O_3 and CO, pollutants that have strong secondary sources, maximize at 20-30% in the tropics. As expected, the NO_x tropospheric load is mostly affected by biomass burning both in the extra-tropics since fires contribute by 50% to the NO_x load at the outflow of boreal fires and in the tropical regions of south America, Africa and N. Australia where burning is significant (Fig. 7c) in agreement with previous studies that show up to 75% reduction near equatorial Africa (Galanter et al., 2000). As a consequence of the NO_x and O_3 reductions when fire emissions are omitted, the computed hydroxyl radical (OH) load (Fig. 7e) is significantly reduced (5-10%) over the same regions; while larger percent reductions are computed at high northern latitudes where OH loads are generally very low due to the very weak photochemistry there.

4.3.2 Impact of injection height

The effect of height distribution of wildfire emissions on the computed tropospheric loads has been studied by comparing the simulations SX.0 with the respective simulations SX.1. Fig. 8 presents such comparisons for BC. Both OC and BC are strongly affected by the injection height parameterization, since emitting aerosols above the boundary layer reduces aerosols available near the surface for loss via dry deposition. The largest differences are computed for the high latitudes over N. America and China where emission height distribution assumptions can result in differences of about 25% (Fig. 8). Previous studies conducted with the GEOS-Chem model over the south eastern Asia during 2001, show a decrease of 20-40% of BC surface concentrations when injected at height (Jian and Fu, 2014). In the same study it is shown that biomass burning injection height has much larger impact on BC than CO (50%-150% more BC calculated at 700hPa, than when emitted in the boundary layer). Differences are positive over source areas (since more is emitted near the surface in SX.1) and negative downwind (since less is transported away from source regions due to the increased deposition flux at the source regions). Additional comparisons are presented in the supplementary material (Fig. S6a-f). Assumptions in the biomass burning emissions injection height marginally affect CO and O_3, with computed differences in the global annual mean tropospheric load smaller than 2.5%.

4.3.3 Chemical feedbacks between biomass burning and vegetation emissions

It is interesting to examine the impact of wildfire emissions on isoprene tropospheric load. Isoprene is the single most important biogenic volatile organic compound (BVOC) emitted by vegetation (more than 50% of total annual BVOC emissions). The changes in OH described in section 4.3.1 (Fig. 7e), the main tropospheric oxidant that consumes isoprene, led to opposite in sign changes of isoprene (Fig. 7f). Such results indicate a strong chemical feedback between biomass burning and species emitted by vegetation.

This feedback is linking isoprene destruction and aerosol formation via the oxidants (hydroxyl-OH- and nitrate-NO_3- radicals and ozone) that consume isoprene and produce semi-volatile organics but also via primary biomass burning aerosols that provide surface for organics to condense on. In the presence of fires, for the same isoprene emissions from vegetation (Fig. 7e) more nitrogen oxides (NO_x) (Fig. 7c) are emitted leading to higher OH

radicals in the extended biomass burning region (up to 20% regionally) and slightly lower over northern hemisphere regions with intensive anthropogenic NO_x emissions and their outflow. Thus, isoprene ambient levels are reduced with the highest reduction over and downwind tropical forested areas. Isoprene global tropospheric column is calculated to be lower by 15% in S0.0 than in S4.0 (fig. 7f). However, due to the NO_x-dependence of the semi-volatile organic compounds formation from isoprene oxidation the total isoprene_SOA concentrations change little (1%). This implies an overall 14% reduction in semi-volatile organic compounds formation yield from isoprene oxidation that comes to compensate for the increased isoprene oxidation. In addition, the primary organic aerosols (POA) emitted by biomass burning provide surface for partitioning of semi-volatile compounds, thus significantly increasing the partitioning of organic vapors to the aerosol phase that in turn also stimulate further partitioning to the aerosol phase. Thus, the isoprene-SOA partitioning to the aerosol phase increases by 19% in depletion of the gas phase isoprene-SOA precursors. This enhancement is consistent with, although much lower than derived from results by Kanakidou et al. (2000) on the enhancement of SOA formation from biogenic VOC due to partitioning on POA from pollution sources. That earlier study was using higher aerosol yields from BVOC than here and did not account for the later studied NO_x-dependence of these yields; it also presented changes due to both combustion and fossil fuel POA. It has also shown that the use of different parameters in the two product yield representation of SOA formation from BVOC can lead to up to 70% of differences in the computed SOA tropospheric burden depending on atmospheric conditions. Tsigaridis et al. (2006) have evaluated the importance of the consideration of NO_x-dependent SOA formation by calculating changes in the SOA burden and characteristics and found that in the current troposphere about 72% of the total SOA mass is formed under NO_x-driven chemistry while in the past this fraction was lower (48%). Note however that large uncertainties and gaps in knowledge exist in the kinetics of isoprene-aerosol formation. Rollins et al. (2009) studying the NO_3 radical-driven chemistry of isoprene-SOA formation, have demonstrated the complexity of isoprene chemistry with respect to SOA formation with a drastic increase in aerosol yield when both double bounds of isoprene are oxidized, thus documenting the aerosol yield dependence on the level of oxidation of the precursors. Ervens et al. (2008) investigations have shown that isoprene aqueous phase chemistry is more efficient (about 40% aerosol yield) than gas phase chemistry (about 3% of aerosol yield) in forming SOA and depends on the water content in the

atmosphere and the pH. Carlton et al. (2009) review of laboratory measurements, field experiments and modeling studies concerning SOA formation from isoprene, documented differences in SOA yield parameterizations that most rely on a single set of chamber experiments, while aerosol yields are known to depend on various factors including the relative importance of NO_x versus peroxide chemistry, temperature (that affects aerosol components volatility based on their enthalpy of vaporization) and pre-existing aerosol loading. They have calculated differences in SOA load induced by the NO_x dependence parameterizations that are up to 30% of the total simulated OA over Eastern USA.

This feedback in the presence of biomass burning emissions increases by about 40% the global mean apparent aerosol yield from isoprene that is defined as the ratio of the tropospheric load of secondary organic aerosol from isoprene oxidation to the tropospheric load of isoprene itself. Impacts on the apparent yields of the first generation gaseous products of isoprene are smaller, i.e. of the order of 7-8%. The supplementary figure S11 shows the spatial distribution of the percent changes in the apparent aerosol yield from isoprene as computed comparing simulations S4.0 and S0.0. This figure points to the areas where the impact of biomass burning emissions (in percent) on the apparent SOA yield from isoprene is calculated by our model to be significant. These areas are the high latitude zone of North America and Asia, the tropical regions over land as well as the outflow from biomass burning regions. Note however that most isoprene_SOA formation occurs over land.

Our results demonstrate the strong coupling between tropospheric chemistry, biomass burning and vegetation emitted species. They show that it is critical for the evaluation of the impact of these emissions on tropospheric chemistry to consistently account for BVOC emissions from vegetation and the co-location/co-occurrence of biomass burning emissions in the area. Co-location of vegetation and biomass burning emissions is linked to the model grid size since co-location area increases with lowering the horizontal resolution of the model. In this respect, to further investigate the impact of the feedback strength to the model resolution, a lower resolution set of simulations has been also performed. These low resolution simulations give results similar to the higher resolution with regard to the feedback strength (relative changes between S0.0 and S4.0). Thus, the percent increases do not seem to be affected by the resolution of the model, while the computed tropospheric loads of isoprene and secondary organic aerosol differ between the high and low resolution simulations with low resolution simulation computing about 10% lower SOA and 4% lower isoprene loads.

4.4 Tropospheric lifetimes

The lifetimes of pollutants provide a measure of pollutant persistence in the atmosphere. They are here computed as the ratio of the tropospheric load to the loss rate (sum of chemical loss and deposition fluxes) for each model column (first 22 vertical layers of the model). Global mean tropospheric lifetimes are derived from the computed global burdens and losses. Changes in chemistry as discussed above, as well as changes in deposition of pollutants due to the modification of their spatial distribution, affect the lifetime of these compounds in the troposphere. Thus, isoprene's lifetime is increased in S4.0, as previously explained, by almost 20% compared to S0.0. The global tropospheric lifetimes of all other species are less impacted by the choice of the emission inventory, with a maximum of about 12% for OC. This is in agreement with previously calculated differences reported in literature. For instance, such differences resulting from the use of 3 different biomass burning inventories (two global and one regional) in the TM4 model coupled with the CBM4 chemical mechanism do not exceed 5% for the African domain (Williams et al. (2012). Table 6 shows the calculated global tropospheric lifetimes of pollutants for each scenario. The maximum percentage differences from the base case scenario (S0.0) are computed for the S4.0 simulation that neglects all wildfire emissions.

The lifetimes of pollutants, computed as the ratio of the tropospheric load to the loss rate (sum of chemical loss and deposition fluxes) for each model column, show sensitivity to both the height distribution of the emissions and the different emission inventories. The sensitivity of the BC lifetime to the height of injection of the biomass burning emissions is depicted in Fig. 9, where the difference in calculated tropospheric lifetimes of OC attributed to emission injection height alone can reach 30% (right panels). The differences produced by injection height for other species are provided in Fig. S7 (supplement). The use of different biomass burning emission inventories led to up to almost 90% local differences for OC as seen in Fig. 9g. The maximum differences are computed in the tropics and over the boreal forests in Canada and eastern Russia using the ACCMIP and FINN inventories (Fig. 9e,g). The overall impact of biomass burning emissions (simulations S4.0 versus S0.0) on the regional lifetimes of tracers is shown in Fig. 10, where significant increases in O_3 (up to about 25%) and CO (up to about a factor of 2) lifetimes are calculated when wild fire emissions are neglected. Biomass burning is reducing O_3 lifetime in the burning regions of the tropics and the boreal forests. This is mainly due to the reaction of O_3 with NO emissions and subsequent HNO_3

formation. The impact of fire emissions on chemistry can be seen through the increases in the regional lifetime of CO and isoprene in S4.0 (Fig. 10a,d), where local differences can reach 160%. OC and BC lifetimes are highly affected with local computed differences up to almost 90% (OC) and 150% (BC) (Fig. 10e-f). Similar results are produced for SO_4^{2-} lifetimes where the local differences in calculated tropospheric lifetimes range from about -25% to 25% near the tropics (Fig. 10g) and above the boreal forests of Russia and Canada where most open biomass burning events occur. Note that aerosols species like OC and BC have significant primary emissions from biomass burning and are removed from the atmosphere by dry and wet deposition, while carbon monoxide, isoprene and O_3 loads and lifetimes are driven by strong chemical production and loss terms. Thus, aerosol species behave differently than these short lived chemically reactive gases.

The tropospheric NO_y lifetime (NO_y=sum of NO_x, HNO_3, peroxyacetyl nitrate and organic nitrates) strongly responds to the wild fire emissions used in the model, with differences between about -40% and 60%. When wild fire emissions are omitted in the model, the NO_y lifetime is increased by about 75% locally (Fig. 11), although on global scale a smaller lifetime change is computed (Table 6). Fig. 11 depicts large local differences between the different scenarios even in the sign of lifetime changes. Focusing on central Canada and north eastern Asia, the S2.0 simulation results in a large increase in NO_y lifetime compared to S0.0 that is weaker for the S1.0. These differences are mainly attributed to the spatial distribution of the emissions favoring different chemistry pathways and resulting in different dry and wet removal fluxes.

5 Conclusions

The CTM sensitivity simulations performed here show that the choice of wildfire emission inventory has a significant impact on the simulated tropospheric concentrations of both primary emitted and secondary produced species, and as a result on the tropospheric lifetimes of gaseous and aerosol pollutants.

The differences introduced by the choice of biomass burning emissions are usually between -30% and 30% above and downwind of biomass burning hotspots (near the tropics, boreal forests of Russia and Canada) and can reach up to a factor of about 7 (e.g. for BC Fig. S4). These impacts maximize for primary pollutants over source areas and for secondary pollutants

downwind. They are either due to the spatial and temporal differences in the emitted amounts of primary pollutants, or to the resulting changes in the levels of oxidants and thus to the impact of the primary pollutants on the concentrations of the chemically produced or destroyed tracers. The injection height of the wildfire emissions is found to affect both the tropospheric load and the lifetimes of the pollutants. Regionally up to 30% differences are computed in the calculated tropospheric lifetimes of pollutants. Tropospheric column of OC is mostly affected by different emission injection height with regional differences ranging from -20% to 25% and those attributed to the different emission inventories ranging from -70% to 450% (Fig. S8b).

Interestingly, isoprene, mainly emitted by vegetation, shows sensitivity to the biomass burning emissions, with increasing tropospheric concentrations (and lifetime) when fire emissions decrease mainly due to the reduction in OH radical concentrations. This leads to an increase of the global mean apparent aerosol yield from isoprene, defined as the ratio of tropospheric loads of secondary aerosol from isoprene oxidation to that of isoprene, by about 40% when biomass burning emissions are taken into account. This fractional increase shows no sensitivity to the model resolution.

Finally, comparison of model results to observations shows the limitations of current observations in evaluating the biomass burning emission inventories. Such evaluation requires densifying air quality monitoring close to and downwind the major biomass burning sources in the tropics, as well as over boreal regions, Alaska, South Asia and Indonesia where our simulations using different biomass burning emission inventories show the larger diversity.

6 Acknowledgements

This work has been supported by the EU-FP7 project ECLIPSE (FP7-ENV-2011-282688). ND acknowledges support from the EU-FP7 project PEGASOS (FP7-ENV-2010-265148). The authors would like to the thank the reviewers for their pertinent comments that helped improving this work.

References

Akagi, S. K., Yokelson, R. J., Wiedinmyer, C., Alvarado, M. J., Reid, J. S., Karl, T., Crounse, J. D., and Wennberg, P. O.: Emission factors for open and domestic biomass burning for use in atmospheric models, Atmos. Chem. Phys., 11, 4039-4072, doi: 10.5194/acp-11-4039-2011, 2011.

Andreae, M. O. and Merlet, P.: Emission of trace gases and aerosols from biomass burning, Global Biogeochem. Cy., 15, 955-966, doi: 10.1029/2000GB001382, 2001.

Beer, R., Glavich, T. A., and Rider, D. M.: Tropospheric emission spectrometer for the Earth Observing System?s Aura satellite, Appl. Opt., 40, 2356-2367, doi: 10.1364/AO.40.002356, 2001.

Bond, T. C., Streets, D. G., Yarber, K. F., Nelson, S. M., Woo, J.-H., and Klimont, Z.: A technology-based global inventory of black and organic carbon emissions from combustion, J. Geophys. Res.-Atmos., 109, D14203, doi: 10.1029/2003JD003697, 2004.

Carlton, A. G., Wiedinmyer, C., and Kroll, J. H.: A review of Secondary Organic Aerosol (SOA) formation from isoprene, Atmos. Chem. Phys., 9, 4987-5005, doi: 10.5194/acp-9-4987-2009, 2009.

Chatfield, R. B. and Delany, A. C.: Convection links biomass burning to increased tropical ozone: However, models will tend to overpredict O3, J. Geophys. Res.-Atmos., 95, 18473-18488, doi: 10.1029/JD095iD11p18473, 1990.

Colarco, P. R., Schoeberl, M. R., Doddridge, B. G., Marufu, L. T., Torres, O., and Welton, E. J.: Transport of smoke from Canadian forest fires to the surface near Washington, D.C.: Injection height, entrainment, and optical properties, J. Geophys. Res.-Atmos., 109, D06203, doi: 10.1029/2003JD004248, 2004.

Crounse, J. D., DeCarlo, P. F., Blake, D. R., Emmons, L. K., Campos, T. L., Apel, E. C., Clarke, A. D., Weinheimer, A. J., McCabe, D. C., Yokelson, R. J., Jimenez, J. L., and Wennberg, P. O.: Biomass burning and urban air pollution over the Central Mexican Plateau, Atmos. Chem. Phys., 9, 4929-4944, doi: 10.5194/acp-9-4929-2009, 2009.

Crutzen, P. J.: An overview of atmospheric chemistry. In: Topics in Atmospheric and Interstellar Physics and Chemistry, Boutron, C. F. (Ed.), Les Editions de Physique, France, 1994.

Crutzen, P. J. and Andreae, M. O.: Biomass Burning in the Tropics: Impact on Atmospheric Chemistry and Biogeochemical Cycles, Science, 250, 1669-1678, doi: 10.1126/science.250.4988.1669, 1990.

Dee, D. P., Uppala, S. M., Simmons, A. J., Berrisford, P., Poli, P., Kobayashi, S., Andrae, U., Balmaseda, M. A., Balsamo, G., Bauer, P., Bechtold, P., Beljaars, A. C. M., van de Berg, L., Bidlot, J., Bormann, N., Delsol, C., Dragani, R., Fuentes, M., Geer, A. J., Haimberger, L., Healy, S. B., Hersbach, H., Hólm, E. V., Isaksen, L., Kållberg, P., Köhler, M., Matricardi, M., McNally, A. P., Monge-Sanz, B. M., Morcrette, J. J., Park, B. K., Peubey, C., de Rosnay, P., Tavolato, C., Thépaut, J. N., and Vitart, F.: The ERA-Interim reanalysis: configuration and performance of the data assimilation system, Q. J. Roy. Meteor. Soc., 137, 553-597, doi: 10.1002/qj.828, 2011.

Dentener, F., Kinne, S., Bond, T., Boucher, O., Cofala, J., Generoso, S., Ginoux, P., Gong, S., Hoelzemann, J. J., Ito, A., Marelli, L., Penner, J. E., Putaud, J. P., Textor, C., Schulz, M., van der Werf, G. R., and Wilson, J.: Emissions of primary aerosol and precursor gases in the years 2000 and 1750 prescribed data-sets for AeroCom, Atmos. Chem. Phys., 6, 4321-4344, doi: 10.5194/acp-6-4321-2006, 2006.

Dirksen, R. J., Folkert Boersma, K., de Laat, J., Stammes, P., van der Werf, G. R., Val Martin, M., and Kelder, H. M.: An aerosol boomerang: Rapid around-the-world transport of

smoke from the December 2006 Australian forest fires observed from space, J. Geophys. Res.-Atmos., 114, D21201, doi: 10.1029/2009JD012360, 2009.

Duan, F., Liu, X., Yu, T., and Cachier, H.: Identification and estimate of biomass burning contribution to the urban aerosol organic carbon concentrations in Beijing, Atmospheric Environment, 38, 1275-1282, doi: 10.1016/j.atmosenv.2003.11.037, 2004.

Edwards, D. P., Emmons, L. K., Gille, J. C., Chu, A., Attié, J. L., Giglio, L., Wood, S. W., Haywood, J., Deeter, M. N., Massie, S. T., Ziskin, D. C., and Drummond, J. R.: Satellite-observed pollution from Southern Hemisphere biomass burning, J. Geophys. Res.-Atmos., 111, D14312, doi: 10.1029/2005JD006655, 2006.

Ervens, B., Carlton, A. G., Turpin, B. J., Altieri, K. E., Kreidenweis, S. M., and Feingold, G.: Secondary organic aerosol yields from cloud-processing of isoprene oxidation products, Geophysical Research Letters, 35, L02816, doi: 10.1029/2007GL031828, 2008.

Field, R. D., van der Werf, G. R., and Shen, S. S. P.: Human amplification of drought-induced biomass burning in Indonesia since 1960, Nature Geosci, 2, 185-188, doi: 10.1038/ngeo443, 2009.

Fountoukis, C. and Nenes, A.: ISORROPIA II: a computationally efficient thermodynamic equilibrium model for K^+ - Ca^{2+}-Mg^{2+}- NH_4^+ - Na^+- SO_4^{2-} - NO_3^- - Cl^- - H_2O aerosols, Atmos. Chem. Phys., 7, 4639-4659, doi: 10.5194/acp-7-4639-2007, 2007.

Freitas, S. R., Longo, K. M., Chatfield, R., Latham, D., Silva Dias, M. A. F., Andreae, M. O., Prins, E., Santos, J. C., Gielow, R., and Carvalho Jr, J. A.: Including the sub-grid scale plume rise of vegetation fires in low resolution atmospheric transport models, Atmos. Chem. Phys., 7, 3385-3398, doi: 10.5194/acp-7-3385-2007, 2007.

Fromm, M., Alfred, J., Hoppel, K., Hornstein, J., Bevilacqua, R., Shettle, E., Servranckx, R., Li, Z., and Stocks, B.: Observations of boreal forest fire smoke in the stratosphere by POAM III, SAGE II, and lidar in 1998, Geophys. Res. Lett., 27, 1407-1410, doi: 10.1029/1999GL011200, 2000.

Galanter, M., Levy, H., and Carmichael, G. R.: Impacts of biomass burning on tropospheric CO, NO x , and O3, J. Geophys. Res.-Atmos., 105, 6633-6653, doi: 10.1029/1999JD901113, 2000.

Granier, C., Bessagnet, B., Bond, T., D'Angiola, A., Denier van der Gon, H., Frost, G., Heil, A., Kaiser, J., Kinne, S., Klimont, Z., Kloster, S., Lamarque, J.-F., Liousse, C., Masui, T., Meleux, F., Mieville, A., Ohara, T., Raut, J.-C., Riahi, K., Schultz, M., Smith, S., Thompson, A., van Aardenne, J., van der Werf, G., and van Vuuren, D.: Evolution of anthropogenic and biomass burning emissions of air pollutants at global and regional scales during the 1980–2010 period, Climatic Change, 109, 163-190, doi: 10.1007/s10584-011-0154-1, 2011.

Guan, H., Chatfield, R. B., Freitas, S. R., Bergstrom, R. W., and Longo, K. M.: Modeling the effect of plume-rise on the transport of carbon monoxide over Africa with NCAR CAM, Atmos. Chem. Phys., 8, 6801-6812, doi: 10.5194/acp-8-6801-2008, 2008.

Guenther, A. B., Jiang, X., Heald, C. L., Sakulyanontvittaya, T., Duhl, T., Emmons, L. K., and Wang, X.: The Model of Emissions of Gases and Aerosols from Nature version 2.1 (MEGAN2.1): an extended and updated framework for modeling biogenic emissions, Geosci. Model Dev., 5, 1471-1492, doi: 10.5194/gmd-5-1471-2012, 2012.

Hodzic, A., Vautard, R., Chepfer, H., Goloub, P., Menut, L., Chazette, P., Deuzé, J. L., Apituley, A., and Couvert, P.: Evolution of aerosol optical thickness over Europe during the August 2003 heat wave as seen from CHIMERE model simulations and POLDER data, Atmos. Chem. Phys., 6, 1853-1864, doi: 10.5194/acp-6-1853-2006, 2006.

Honrath, R. E., Owen, R. C., Martin, M. V., Reid, J. S., Lapina, K., Fialho, P., Dziobak, M. P., Kleissl, J., and Westphal, D. L.: Regional and hemispheric impacts of anthropogenic and biomass burning emissions on summertime CO and O3in the North Atlantic lower free troposphere, J. Geophys. Res.-Atmos., 109, doi: 10.1029/2004jd005147, 2004.

Jaffe, D., Bertschi, I., Jaeglé, L., Novelli, P., Reid, J. S., Tanimoto, H., Vingarzan, R., and Westphal, D. L.: Long-range transport of Siberian biomass burning emissions and impact on surface ozone in western North America, Geophys. Res. Lett., 31, L16106, doi: 10.1029/2004GL020093, 2004.

Jaffe, D. A. and Wigder, N. L.: Ozone production from wildfires: A critical review, Atmos. Environ., 51, 1-10, doi: 10.1016/j.atmosenv.2011.11.063, 2012.

Jian, Y. and Fu, T. M.: Injection heights of springtime biomass-burning plumes over peninsular Southeast Asia and their impacts on long-range pollutant transport, Atmos. Chem. Phys., 14, 3977-3989, doi: 10.5194/acp-14-3977-2014, 2014.

Kaiser, J. W., Heil, A., Andreae, M. O., Benedetti, A., Chubarova, N., Jones, L., Morcrette, J. J., Razinger, M., Schultz, M. G., Suttie, M., and van der Werf, G. R.: Biomass burning emissions estimated with a global fire assimilation system based on observed fire radiative power, Biogeosciences, 9, 527-554, doi: 10.5194/bg-9-527-2012, 2012.

Kanakidou, M. and Crutzen, P. J.: The photochemical source of carbon monoxide: Importance, uncertainties and feedbacks, Chemosphere - Global Change Science, 1, 91-109, doi: 10.1016/S1465-9972(99)00022-7, 1999.

Kanakidou, M., Duce, R. A., Prospero, J. M., Baker, A. R., Benitez-Nelson, C., Dentener, F. J., Hunter, K. A., Liss, P. S., Mahowald, N., Okin, G. S., Sarin, M., Tsigaridis, K., Uematsu, M., Zamora, L. M., and Zhu, T.: Atmospheric fluxes of organic N and P to the global ocean, Global Biogeochem. Cy., 26, GB3026, doi: 10.1029/2011GB004277, 2012.

Kanakidou, M., Tsigaridis, K., Dentener, F. J., and Crutzen, P. J.: Human-activity-enhanced formation of organic aerosols by biogenic hydrocarbon oxidation, Journal of Geophysical Research: Atmospheres, 105, 9243-9354, doi: 10.1029/1999JD901148, 2000.

Keywood, M., Kanakidou, M., Stohl, A., Dentener, F., Grassi, G., Meyer, C. P., Torseth, K., Edwards, D., Thompson, A. M., Lohmann, U., and Burrows, J.: Fire in the Air: Biomass Burning Impacts in a Changing Climate, Crit. Rev. Env. Sci. Tec., 43, 40-83, doi: 10.1080/10643389.2011.604248, 2013.

Klimont, Z., Smith, S. J., and Cofala, J.: The last decade of global anthropogenic sulfur dioxide: 2000–2011 emissions, Environ. Res. Lett., 8, 014003, doi: 10.1088/1748-9326/8/1/014003, 2013.

Lamarque, J. F., Shindell, D. T., Josse, B., Young, P. J., Cionni, I., Eyring, V., Bergmann, D., Cameron-Smith, P., Collins, W. J., Doherty, R., Dalsoren, S., Faluvegi, G., Folberth, G., Ghan, S. J., Horowitz, L. W., Lee, Y. H., MacKenzie, I. A., Nagashima, T., Naik, V., Plummer, D., Righi, M., Rumbold, S. T., Schulz, M., Skeie, R. B., Stevenson, D. S., Strode, S., Sudo, K., Szopa, S., Voulgarakis, A., and Zeng, G.: The Atmospheric Chemistry and Climate Model Intercomparison Project (ACCMIP): overview and description of models,

simulations and climate diagnostics, Geosci. Model Dev., 6, 179-206, doi: 10.5194/gmd-6-179-2013, 2013.

Lavoué, D., Liousse, C., Cachier, H., Stocks, B. J., and Goldammer, J. G.: Modeling of carbonaceous particles emitted by boreal and temperate wildfires at northern latitudes, J. Geophys. Res.-Atmos., 105, 26871-26890, doi: 10.1029/2000JD900180, 2000.

Lelieveld, J., van Aardenne, J., Fischer, H., de Reus, M., Williams, J., and Winkler, P.: Increasing Ozone over the Atlantic Ocean, Science, 304, 1483-1487, doi: 10.1126/science.1096777, 2004.

Leung, F.-Y. T., Logan, J. A., Park, R., Hyer, E., Kasischke, E., Streets, D., and Yurganov, L.: Impacts of enhanced biomass burning in the boreal forests in 1998 on tropospheric chemistry and the sensitivity of model results to the injection height of emissions, J. Geophys. Res.-Atmos., 112, D10313, doi: 10.1029/2006JD008132, 2007.

Levine, J. S., Cofer, W. R., Cahoon, D. R., and Winstead, E. L.: A DRIVER FOR GLOBAL CHANGE, Environ. Sci. Technol., 29, 120A-125A, doi: 10.1021/es00003a746, 1995.

Mutch, R. W.: Fighting Fire with Prescribed Fire: A Return to Ecosystem Health, J. Forest., 92, 31-33, 1994.

Myriokefalitakis, S., Tsigaridis, K., Mihalopoulos, N., Sciare, J., Nenes, A., Kawamura, K., Segers, A., and Kanakidou, M.: In-cloud oxalate formation in the global troposphere: a 3-D modeling study, Atmos. Chem. Phys., 11, 5761-5782, doi: 10.5194/acp-11-5761-2011, 2011.

Myriokefalitakis, S., Vignati, E., Tsigaridis, K., Papadimas, C., Sciare, J., Mihalopoulos, N., Facchini, M. C., Rinaldi, M., Dentener, F. J., Ceburnis, D., Hatzianastasiou, N., O'Dowd, C. D., van Weele, M., and Kanakidou, M.: Global Modeling of the Oceanic Source of Organic Aerosols, Advances in Meteorology, 2010, 1-16, doi: 10.1155/2010/939171, 2010.

Nenes, A., Pandis, S., and Pilinis, C.: ISORROPIA: A New Thermodynamic Equilibrium Model for Multiphase Multicomponent Inorganic Aerosols, Aquatic Geochemistry, 4, 123-152, doi: 10.1023/A:1009604003981, 1998.

Palmer, P. I., Parrington, M., Lee, J. D., Lewis, A. C., Rickard, A. R., Bernath, P. F., Duck, T. J., Waugh, D. L., Tarasick, D. W., Andrews, S., Aruffo, E., Bailey, L. J., Barrett, E., Bauguitte, S. J. B., Curry, K. R., Di Carlo, P., Chisholm, L., Dan, L., Forster, G., Franklin, J. E., Gibson, M. D., Griffin, D., Helmig, D., Hopkins, J. R., Hopper, J. T., Jenkin, M. E., Kindred, D., Kliever, J., Le Breton, M., Matthiesen, S., Maurice, M., Moller, S., Moore, D. P., Oram, D. E., O'Shea, S. J., Owen, R. C., Pagniello, C. M. L. S., Pawson, S., Percival, C. J., Pierce, J. R., Punjabi, S., Purvis, R. M., Remedios, J. J., Rotermund, K. M., Sakamoto, K. M., da Silva, A. M., Strawbridge, K. B., Strong, K., Taylor, J., Trigwell, R., Tereszchuk, K. A., Walker, K. A., Weaver, D., Whaley, C., and Young, J. C.: Quantifying the impact of BOReal forest fires on Tropospheric oxidants over the Atlantic using Aircraft and Satellites (BORTAS) experiment: design, execution and science overview, Atmos. Chem. Phys., 13, 6239-6261, doi: 10.5194/acp-13-6239-2013, 2013.

Parrington, M., Palmer, P. I., Lewis, A. C., Lee, J. D., Rickard, A. R., Di Carlo, P., Taylor, J. W., Hopkins, J. R., Punjabi, S., Oram, D. E., Forster, G., Aruffo, E., Moller, S. J., Bauguitte, S. J. B., Allan, J. D., Coe, H., and Leigh, R. J.: Ozone photochemistry in boreal biomass burning plumes, Atmos. Chem. Phys., 13, 7321-7341, doi: 10.5194/acp-13-7321-2013, 2013.

Petrenko, M., Kahn, R., Chin, M., Soja, A., Kucsera, T., and Harshvardhan: The use of satellite-measured aerosol optical depth to constrain biomass burning emissions source

strength in the global model GOCART, Journal of Geophysical Research: Atmospheres, 117, D18212, doi: 10.1029/2012JD017870, 2012.

Pfister, G., Hess, P. G., Emmons, L. K., Lamarque, J. F., Wiedinmyer, C., Edwards, D. P., Pétron, G., Gille, J. C., and Sachse, G. W.: Quantifying CO emissions from the 2004 Alaskan wildfires using MOPITT CO data, Geophys. Res. Lett., 32, L11809, doi: 10.1029/2005GL022995, 2005.

Praplan, A. P., Barmet, P., Dommen, J., and Baltensperger, U.: Cyclobutyl methyl ketone as a model compound for pinonic acid to elucidate oxidation mechanisms, Atmos. Chem. Phys., 12, 10749-10758, doi: 10.5194/acp-12-10749-2012, 2012.

Reid, J. S., Eck, T. F., Christopher, S. A., Koppmann, R., Dubovik, O., Eleuterio, D. P., Holben, B. N., Reid, E. A., and Zhang, J.: A review of biomass burning emissions part III: intensive optical properties of biomass burning particles, Atmos. Chem. Phys., 5, 827-849, doi: 10.5194/acp-5-827-2005, 2005.

Rollins, A. W., Kiendler-Scharr, A., Fry, J. L., Brauers, T., Brown, S. S., Dorn, H. P., Dubé, W. P., Fuchs, H., Mensah, A., Mentel, T. F., Rohrer, F., Tillmann, R., Wegener, R., Wooldridge, P. J., and Cohen, R. C.: Isoprene oxidation by nitrate radical: alkyl nitrate and secondary organic aerosol yields, Atmos. Chem. Phys., 9, 6685-6703, doi: 10.5194/acp-9-6685-2009, 2009.

Rosenfeld, D.: TRMM observed first direct evidence of smoke from forest fires inhibiting rainfall, Geophys. Res. Lett., 26, 3105-3108, doi: 10.1029/1999GL006066, 1999.

Simmonds, P. G., Manning, A. J., Derwent, R. G., Ciais, P., Ramonet, M., Kazan, V., and Ryall, D.: A burning question. Can recent growth rate anomalies in the greenhouse gases be attributed to large-scale biomass burning events?, Atmos. Environ., 39, 2513-2517, doi: 10.1016/j.atmosenv.2005.02.018, 2005.

Sindelarova, K., Granier, C., Bouarar, I., Guenther, A., Tilmes, S., Stavrakou, T., Müller, J. F., Kuhn, U., Stefani, P., and Knorr, W.: Global data set of biogenic VOC emissions calculated by the MEGAN model over the last 30 years, Atmos. Chem. Phys., 14, 9317-9341, doi: 10.5194/acp-14-9317-2014, 2014.

Sofiev, M., Ermakova, T., and Vankevich, R.: Evaluation of the smoke-injection height from wild-land fires using remote-sensing data, Atmos. Chem. Phys., 12, 1995-2006, doi: 10.5194/acp-12-1995-2012, 2012.

Sofiev, M., Vankevich, R., Ermakova, T., and Hakkarainen, J.: Global mapping of maximum emission heights and resulting vertical profiles of wildfire emissions, Atmos. Chem. Phys., 13, 7039-7052, doi: 10.5194/acp-13-7039-2013, 2013.

Tsigaridis, K., Daskalakis, N., Kanakidou, M., Adams, P. J., Artaxo, P., Bahadur, R., Balkanski, Y., Bauer, S. E., Bellouin, N., Benedetti, A., Bergman, T., Berntsen, T. K., Beukes, J. P., Bian, H., Carslaw, K. S., Chin, M., Curci, G., Diehl, T., Easter, R. C., Ghan, S. J., Gong, S. L., Hodzic, A., Hoyle, C. R., Iversen, T., Jathar, S., Jimenez, J. L., Kaiser, J. W., Kirkevåg, A., Koch, D., Kokkola, H., Lee, Y. H., Lin, G., Liu, X., Luo, G., Ma, X., Mann, G. W., Mihalopoulos, N., Morcrette, J. J., Müller, J. F., Myhre, G., Myriokefalitakis, S., Ng, S., O'Donnell, D., Penner, J. E., Pozzoli, L., Pringle, K. J., Russell, L. M., Schulz, M., Sciare, J., Seland, Ø., Shindell, D. T., Sillman, S., Skeie, R. B., Spracklen, D., Stavrakou, T., Steenrod, S. D., Takemura, T., Tiitta, P., Tilmes, S., Tost, H., van Noije, T., van Zyl, P. G., von Salzen, K., Yu, F., Wang, Z., Wang, Z., Zaveri, R. A., Zhang, H., Zhang, K., Zhang, Q., and Zhang,

X.: The AeroCom evaluation and intercomparison of organic aerosol in global models, Atmos. Chem. Phys. Discuss., 14, 6027-6161, doi: 10.5194/acpd-14-6027-2014, 2014.

Tsigaridis, K. and Kanakidou, M.: Global modelling of secondary organic aerosol in the troposphere: a sensitivity analysis, Atmos. Chem. Phys., 3, 1849-1869, doi: 10.5194/acp-3-1849-2003, 2003.

Tsigaridis, K. and Kanakidou, M.: Secondary organic aerosol importance in the future atmosphere, Atmos. Environ., 41, 4682-4692, doi: 10.1016/j.atmosenv.2007.03.045, 2007.

Tsigaridis, K., Krol, M., Dentener, F. J., Balkanski, Y., Lathière, J., Metzger, S., Hauglustaine, D. A., and Kanakidou, M.: Change in global aerosol composition since preindustrial times, Atmos. Chem. Phys., 6, 5143-5162, doi: 10.5194/acp-6-5143-2006, 2006.

Val Martin, M., Kahn, R. A., Logan, J. A., Paugam, R., Wooster, M., and Ichoku, C.: Space-based observational constraints for 1-D fire smoke plume-rise models, J. Geophys. Res.-Atmos., 117, n/a-n/a, doi: 10.1029/2012jd018370, 2012.

Val Martin, M., Logan, J. A., Kahn, R. A., Leung, F. Y., Nelson, D. L., and Diner, D. J.: Smoke injection heights from fires in North America: analysis of 5 years of satellite observations, Atmos. Chem. Phys., 10, 1491-1510, doi: 10.5194/acp-10-1491-2010, 2010.

van der Werf, G. R., Randerson, J. T., Giglio, L., Collatz, G. J., Kasibhatla, P. S., and Arellano Jr, A. F.: Interannual variability in global biomass burning emissions from 1997 to 2004, Atmos. Chem. Phys., 6, 3423-3441, doi: 10.5194/acp-6-3423-2006, 2006.

van der Werf, G. R., Randerson, J. T., Giglio, L., Collatz, G. J., Mu, M., Kasibhatla, P. S., Morton, D. C., DeFries, R. S., Jin, Y., and van Leeuwen, T. T.: Global fire emissions and the contribution of deforestation, savanna, forest, agricultural, and peat fires (1997–2009), Atmos. Chem. Phys., 10, 11707-11735, doi: 10.5194/acp-10-11707-2010, 2010.

Vignati, E., Facchini, M. C., Rinaldi, M., Scannell, C., Ceburnis, D., Sciare, J., Kanakidou, M., Myriokefalitakis, S., Dentener, F., and O'Dowd, C. D.: Global scale emission and distribution of sea-spray aerosol: Sea-salt and organic enrichment, Atmos. Environ., 44, 670-677, doi: 10.1016/j.atmosenv.2009.11.013, 2010.

Voulgarakis, A., Telford, P. J., Aghedo, A. M., Braesicke, P., Faluvegi, G., Abraham, N. L., Bowman, K. W., Pyle, J. A., and Shindell, D. T.: Global multi-year O3-CO correlation patterns from models and TES satellite observations, Atmos. Chem. Phys., 11, 5819-5838, doi: 10.5194/acp-11-5819-2011, 2011.

Wiedinmyer, C., Akagi, S. K., Yokelson, R. J., Emmons, L. K., Al-Saadi, J. A., Orlando, J. J., and Soja, A. J.: The Fire INventory from NCAR (FINN): a high resolution global model to estimate the emissions from open burning, Geosci. Model Dev., 4, 625-641, doi: 10.5194/gmd-4-625-2011, 2011.

Williams, J. E., Weele, M. v., Velthoven, P. F. J. v., Scheele, M. P., Liousse, C., and Werf, G. R. v. d.: The Impact of Uncertainties in African Biomass Burning Emission Estimates on Modeling Global Air Quality, Long Range Transport and Tropospheric Chemical Lifetimes, Atmosphere, 3, 132-163, doi: 10.3390/atmos3010132, 2012.

Ziemke, J. R., Chandra, S., Duncan, B. N., Schoeberl, M. R., Torres, O., Damon, M. R., and Bhartia, P. K.: Recent biomass burning in the tropics and related changes in tropospheric ozone, Geophysical Research Letters, 36, L15819, doi: 10.1029/2009GL039303, 2009.

1

Table 1 Anthropogenic emissions (Tg a^{-1}) used in this study and fraction of emissions that corresponds to the AWB sector included in the ECLIPSE anthropogenic emissions inventory. Both absolute quantities and percentage of the total anthropogenic emissions from (Klimont et al., 2013) are presented.

	BC	CO	NOx	OC	SOx	NMVOC
ECLPSE (with AWB)	5.38	527.1	43.97	11.56	45.95	140.47
AWB on ECLIPSE	0.333	27.46	0.296	1.281	0.173	4.255
% contribution of AWB to total anthropogenic	6.19	5.21	0.67	11.08	0.38	3.03

Table 2 Total annual amounts of pollutants emitted by wild fires according to the different inventories used, for 2008 in Tg a^{-1}. NO_x is reported as NO. (*)GFEDv3.1 without the AWB is here called GFEDv3.1-ECLIPSE

	BC	CO	NO_x	OC	SO_2	NMVOC	NH_3	Spatial resolution	Temporal resolution
GFEDv3.1-ECLIPSE*	1.695	264.205	3.751	15.197	0.940	44.414.	3.320	0.5ºx0.5º	Monthly
FINN	1.939	338.576	5.998	20.202	1.102	63.476	5.410	1ºx1º	Monthly
ACCMIP	2.620	460.419	5.479	23.309	1.929	80.869	9.203	0.5ºx0.5º	Monthly

Table 3 Agricultural Waste Burning sector as provided for different emission inventories in Tg a^{-1} for the year 2008. NOx is reported as NO

	BC	CO	NOx	OC	SOx	NMVOC
ECLIPSE	0.333	27.46	0.296	1.281	0.173	4.255
GFEDv3.1	0.064	12.57	0.143	0.497	0.027	1.296
ACCMIP	0.162	21.22	0.444	0.775	0.220	2.857

Table 4 Summary of simulations performed for this work.

Height	inventory	Varying	Surface	AWB
S0.0	**GFEDv3 ECLIPSE**	**X**		**ECLIPSE**
S0.1			**X**	
S1.0	**GFEDv3.1**	**X**		**GFEDv3.1**
S1.1			**X**	
S2.0	**ACCMIP**	**X**		**ECLIPSE**
S2.1			**X**	
S3.0	**FINN**	**X**		**ECLIPSE**
S3.1			**X**	
S4.0	**zero**			**ECLIPSE**

Table 5 Total annual mean tropospheric load of pollutants for all simulations in Tg a^{-1}.

	S0.0	**S0.1**	**S1.0**	**S1.1**	**S2.0**	**S2.1**	**S3.0**	**S3.1**	**S4.0**
CO	319.12	318.37	317.26	316.20	341.47	339.63	331.58	330.37	283.88
O_3	416.17	415.52	415.35	414.82	422.17	421.29	423.04	422.03	405.25
NO_x	1.299	1.293	1.286	1.282	1.330	1.323	1.390	1.378	1.200
SO_4^{2-}	1.914	1.908	1.913	1.906	1.933	1.923	1.911	1.905	1.868
HNO_3	2.196	2.188	2.181	2.181	2.235	2.228	2.229	2.219	2.048
NH_4^+	0.498	0.487	0.514	0.496	0.516	0.496	0.507	0.492	0.460
Isoprene	0.266	0.267	0.267	0.268	0.247	0.248	0.253	0.254	0.315
OC	0.111	0.110	0.110	0.109	0.121	0.120	0.117	0.116	0.072
BC	0.136	0.135	0.131	0.131	0.146	0.146	0.133	0.133	0.088

Table 6 Calculated annual mean tropospheric lifetimes of pollutants for all the simulations performed.

	S0.0	**S0.1**	**S1.0**	**S1.1**	**S2.0**	**S2.1**	**S3.0**	**S3.1**	**S4.0**
CO (days)	41.48	41.44	41.43	41.35	41.82	41.67	41.45	41.40	41.67
O_3 (days)	24.58	24.62	24.59	24.63	24.39	24.43	24.33	24.39	25.19
NO_y (days)	7.342	7.300	7.293	7.255	7.358	7.297	7.628	7.541	7.184
SO_4^{2-} (days)	4.446	4.442	4.448	4.444	4.427	4.423	4.421	4.419	4.426
HNO_3 (days)	2.804	2.805	2.793	2.800	2.792	2.796	2.774	2.775	2.776
NH_4^+ (days)	4.979	4.932	5.032	4.962	4.961	4.905	4.928	4.894	4.862
Isoprene (hours)	4.457	4.475	4.466	4.482	4.137	4.152	4.236	4.250	5.270
OC (days)	6.031	5.998	6.046	6.012	5.925	5.894	5.839	5.819	5.302
BC (days)	6.927	6.908	6.962	6.941	6.889	6.871	6.583	6.572	6.261

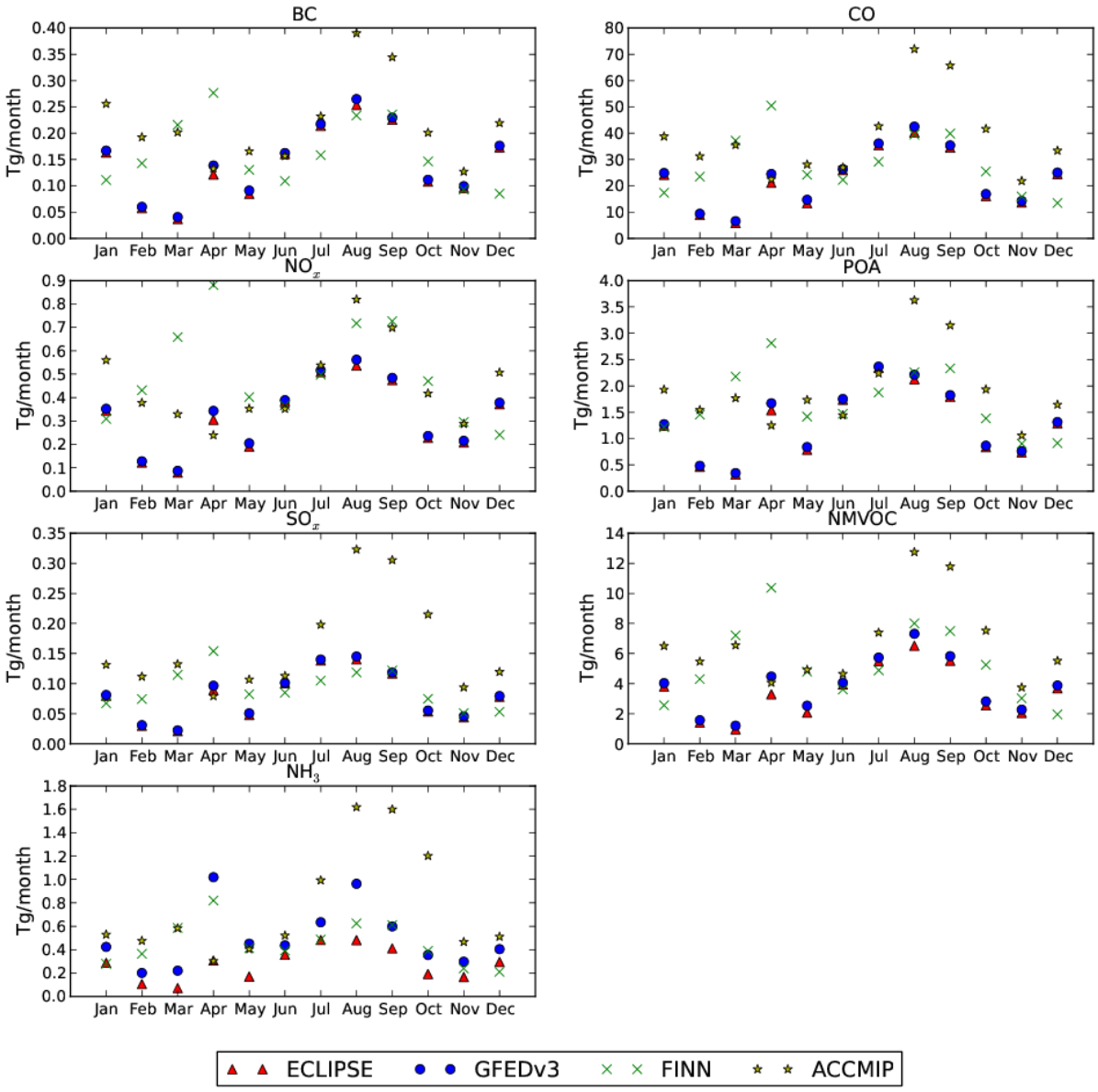

Fig. 1 Monthly variation and differences of biomass burning emission inventories for the year 2008 for all species used in the model. For simplicity, NMVOC are summed up. NOx are presented in NO, SOx in SO_2 and NMVOCs in total mass.

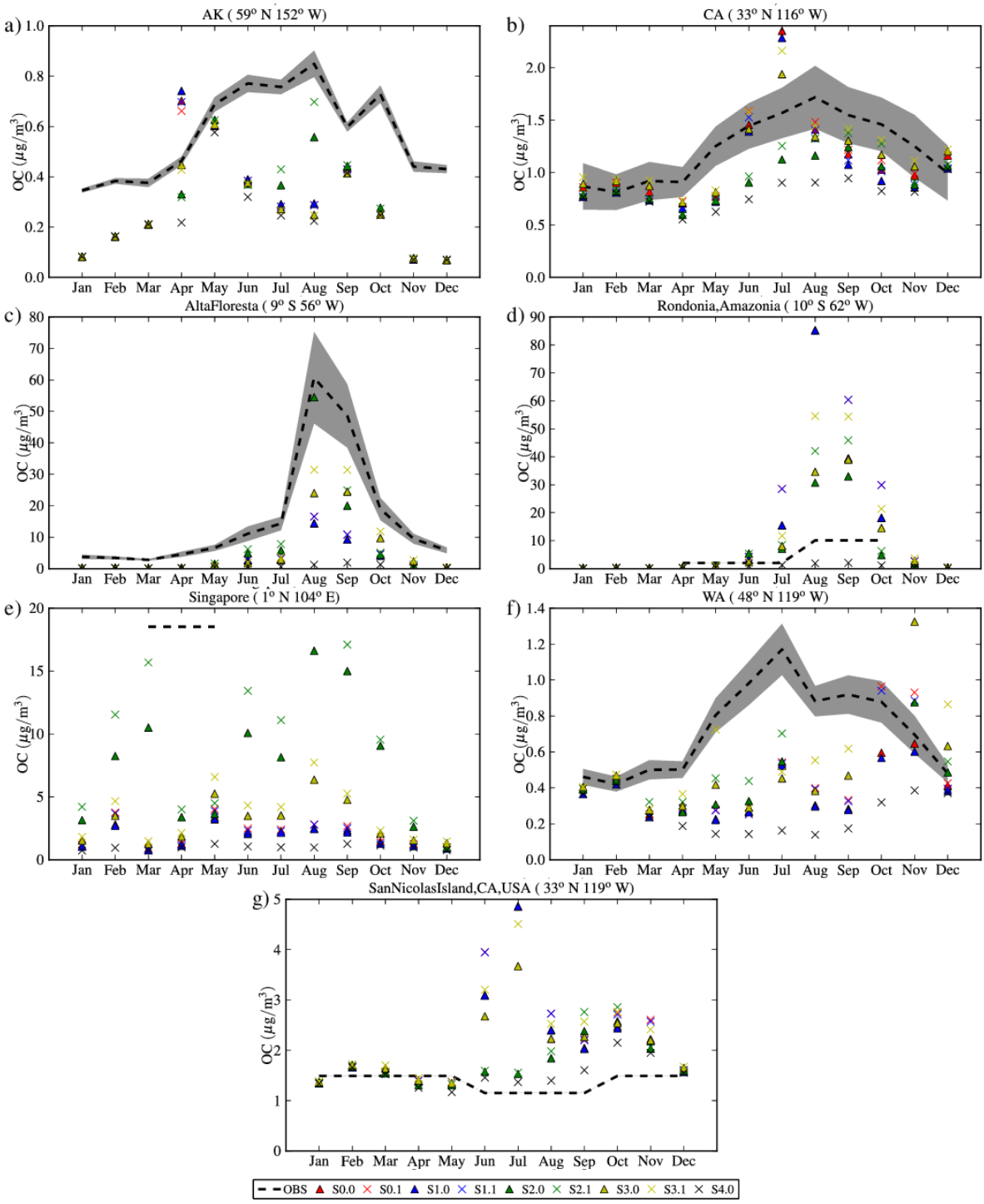

Fig. 2 Comparison of monthly mean model results with observations of organic carbon (OC) at southern Alaska (a), California State, USA (b), Alta Floresta, Brazil (c), Rondonia, Amazonia (d), Singapore (e), Washington State, USA (f) and San Nicolas Island, California, USA (g). The dashed line with the gray shaded area shows the monthly mean value of observations with the standard deviation based on their interannual variability, while the colored symbols show the calculated values for the specific station. Triangles are for simulations assuming a vertical distribution of wildfire emissions, while the x symbols show the simulations assuming that all open biomass burning emissions occur near the surface. Details on the simulations are given in Table 4.

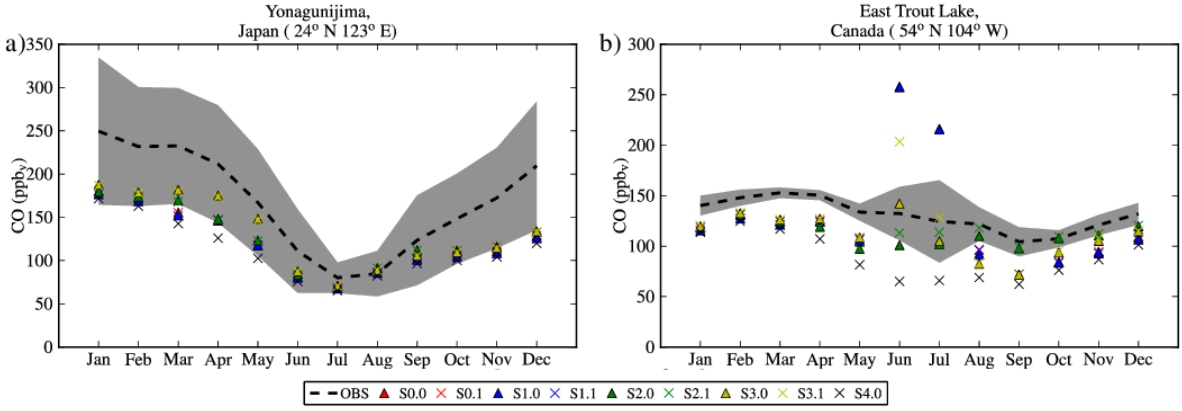

Fig. 3 Comparison of monthly mean model results with CO surface observations at Yonagunijima, Japan (a) and at East Trout Lake, Canada (b). Lines and symbols as in Fig. 2 but for CO.

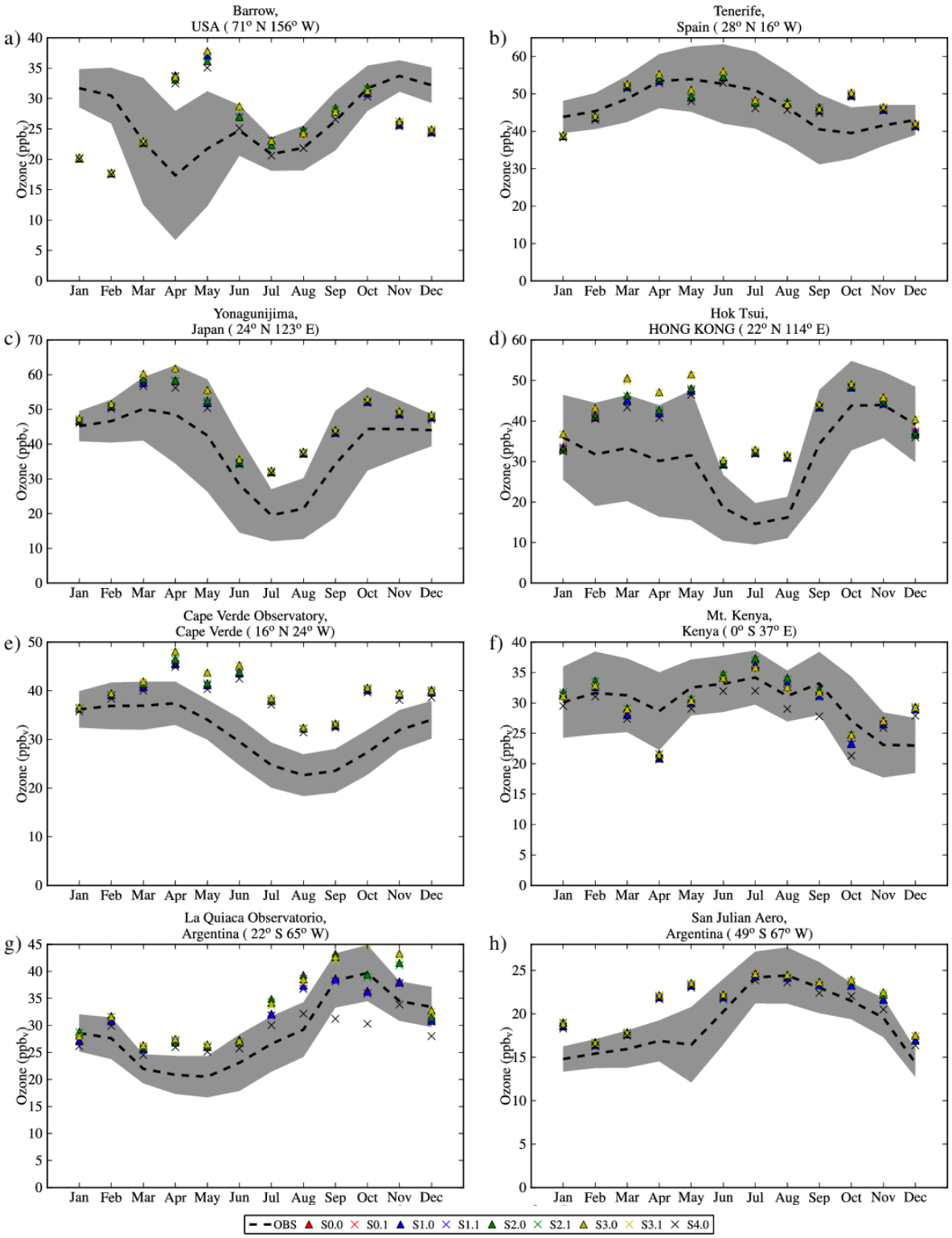

Fig. 4 Comparison of monthly mean surface ozone measurements with model results at Barrow, USA (a), Tenerife, Spain (b), Yonagunijima, Japan (c), Hok Tsui, Hong Kong (d), Cape Verde Observatory, Cape Verde (e), Mount Kenya, Kenya (f), La Quiaca Observatory, Argentina (g) and San Julian Aero, Argentina (h) . Lines and symbols as in Fig. 2 but for O_3.

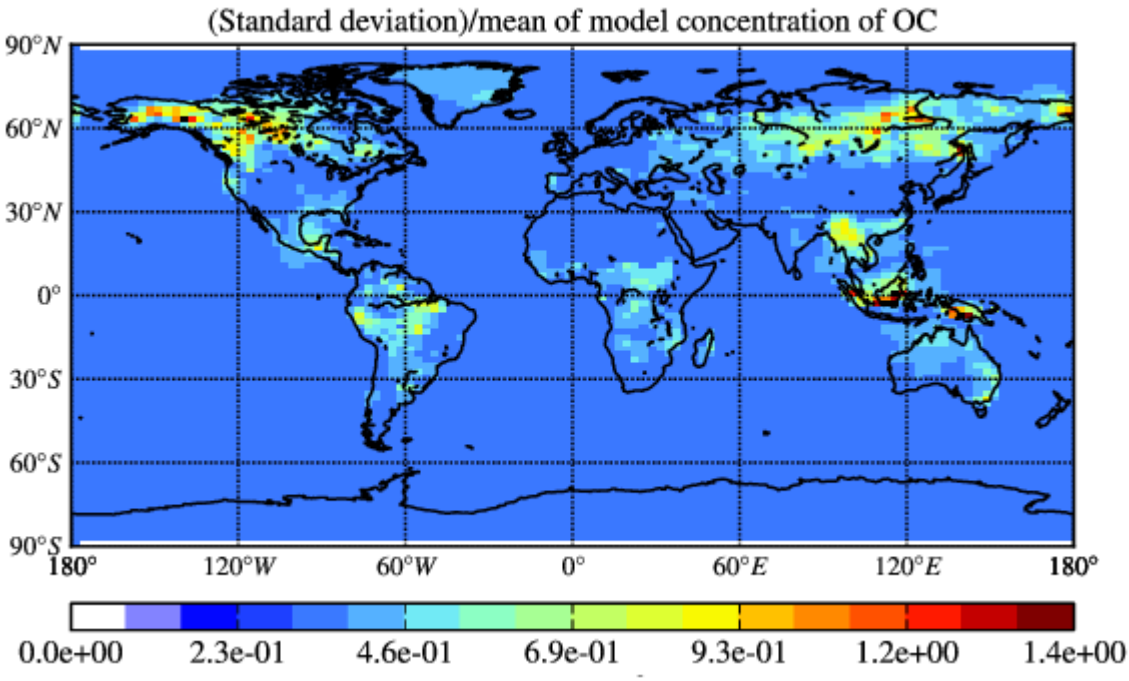

Fig. 5 Spatial distribution of the ratio of the standard deviation to the mean of all model simulations, based on annual mean of the computed surface OC concentrations.

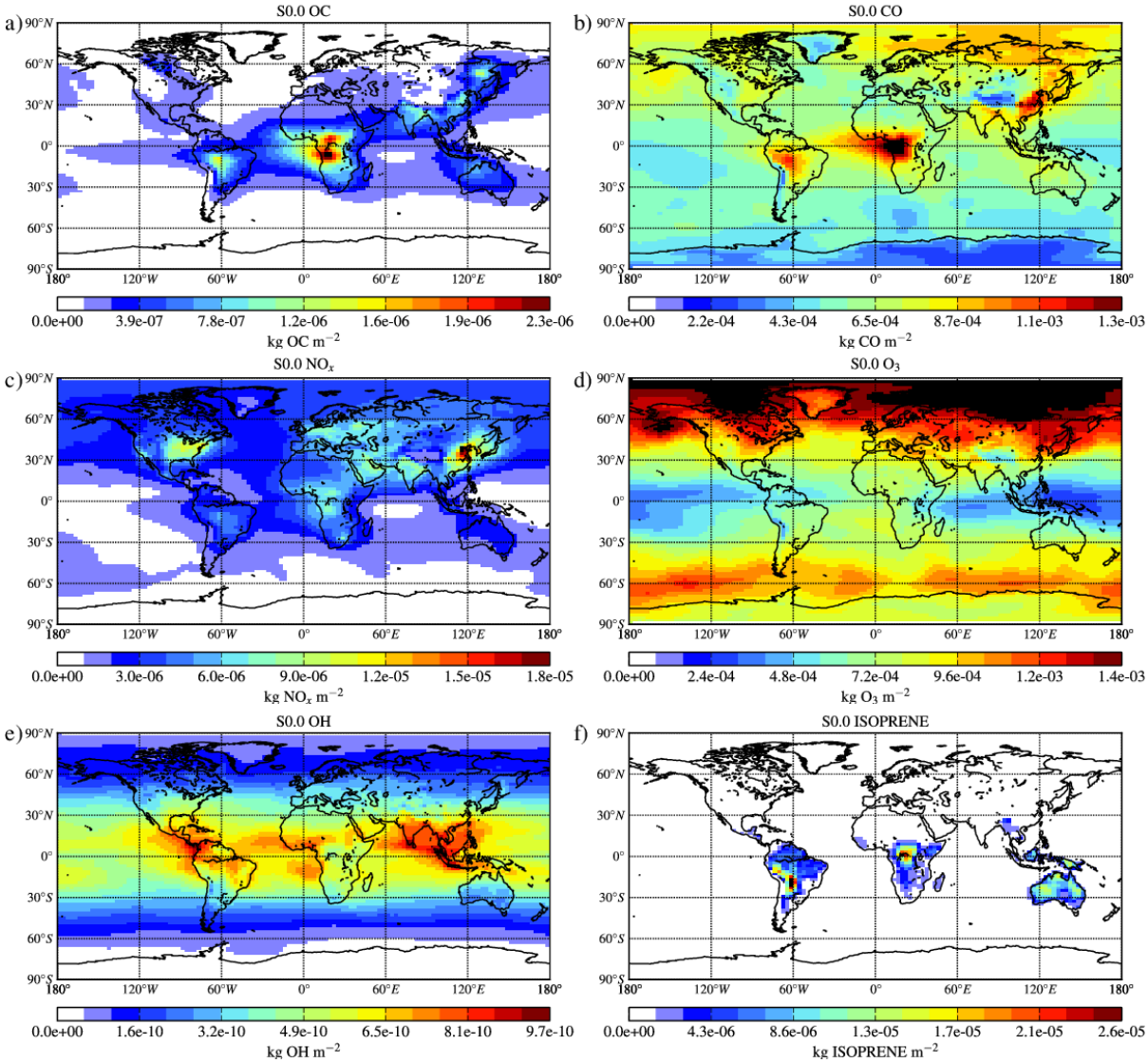

Fig. 6 Calculated annual mean tropospheric load in (Kg m^{-2}) of selected species for the base case scenario (S0.0). Areas with black exceed the maximum value of the colorbar.

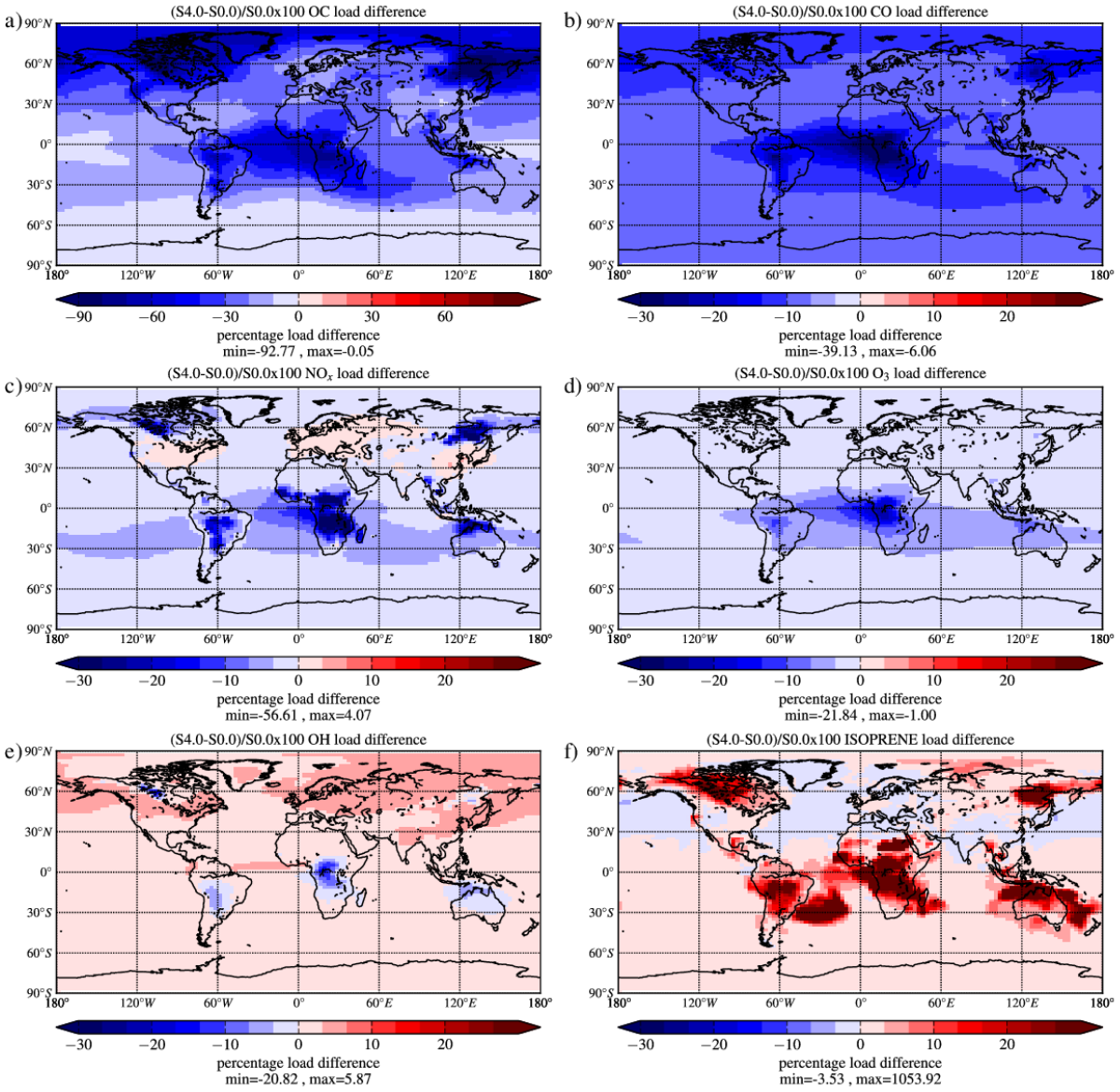

Fig. 7 Percentage difference in the computed annual mean tropospheric loads of OC (a), CO (b), NOx (c), O_3 (d), OH (e), isoprene (f) – attributed to wildfire emissions calculated as (column_S4.0 – column_S0.0)/(column S0.0)x100. The scale is from -30% to 30% (-90% to 90% for OC) ; the minimum and maximum differences are printed under each panel.

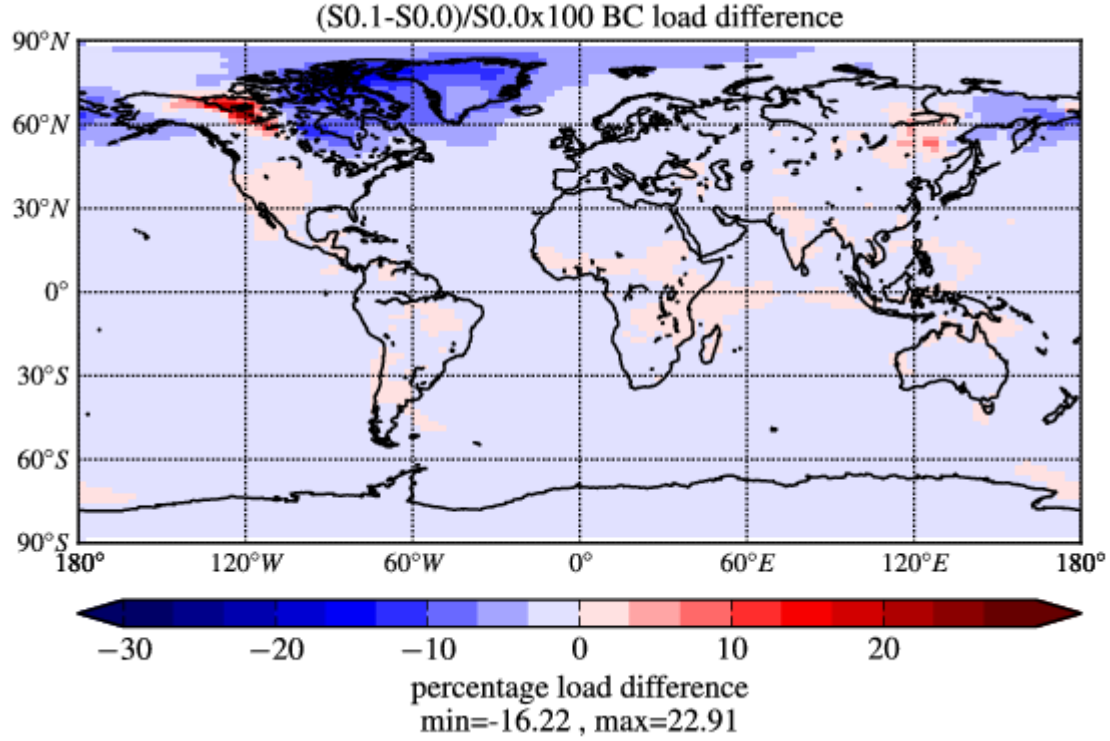

Fig. 8 Percentage difference of annual mean computed tropospheric load of BC attributed to wildfire emission injection height calculated as (load_S0.1 – load_S0.0)/(load S0.0)x100. The scale is from -30% to 30% ; the minimum and maximum percent differences are printed under each panel.

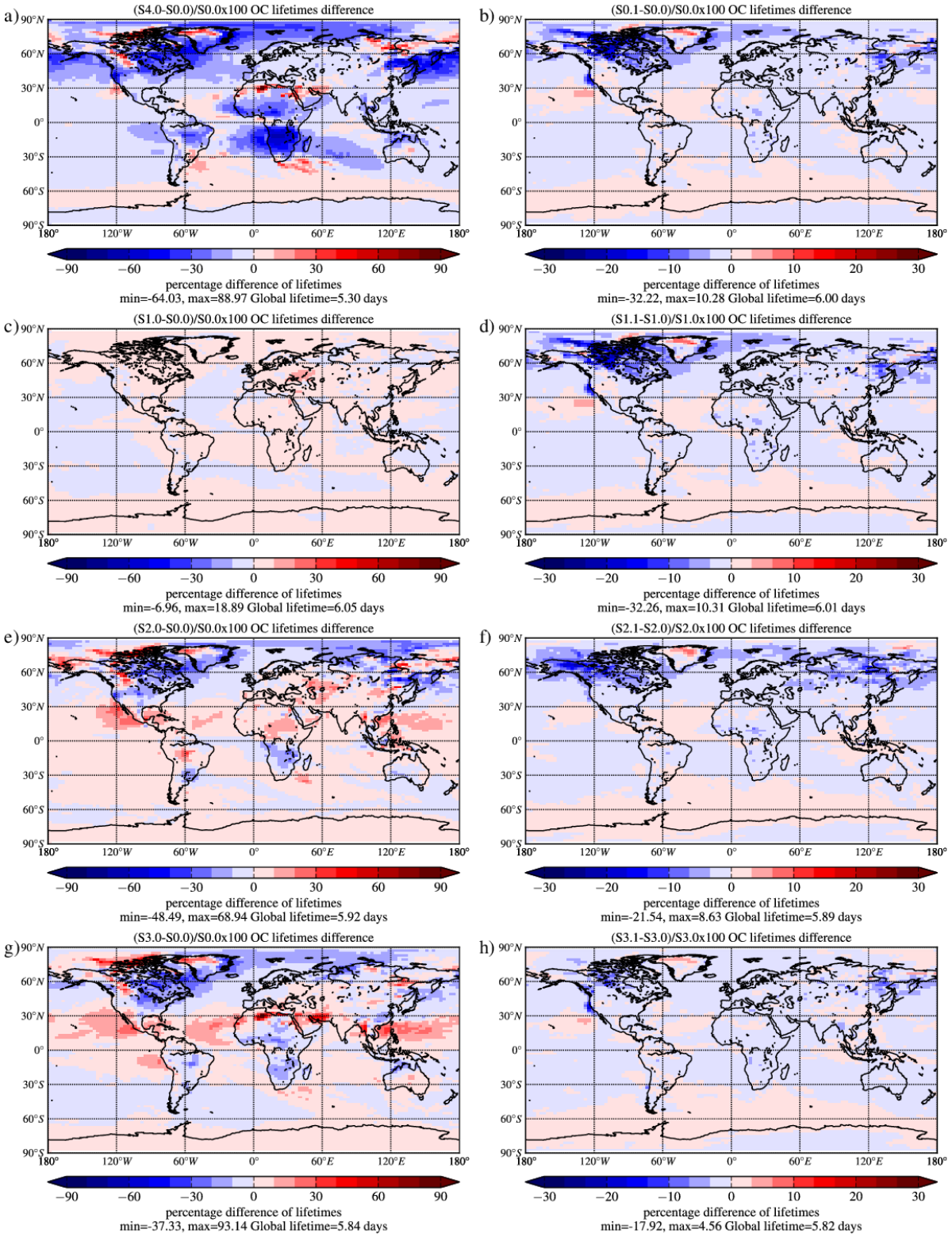

Fig. 9. Percent impact on the computed annual mean tropospheric lifetime of OC of: (left panels) the different emission inventories calculated as the percent difference between simulations SX.0 and simulation S0.0; and of (right panels) height distribution calculated as the percent difference between simulations SX.1 and simulations SX.0.. The colorbar ranges from -90% to 90% for the surface differences and -30% to 30% for the differences induced by height distribution. The minimum and maximum local lifetimes percent changes as well as the global lifetime are printed under each panel.

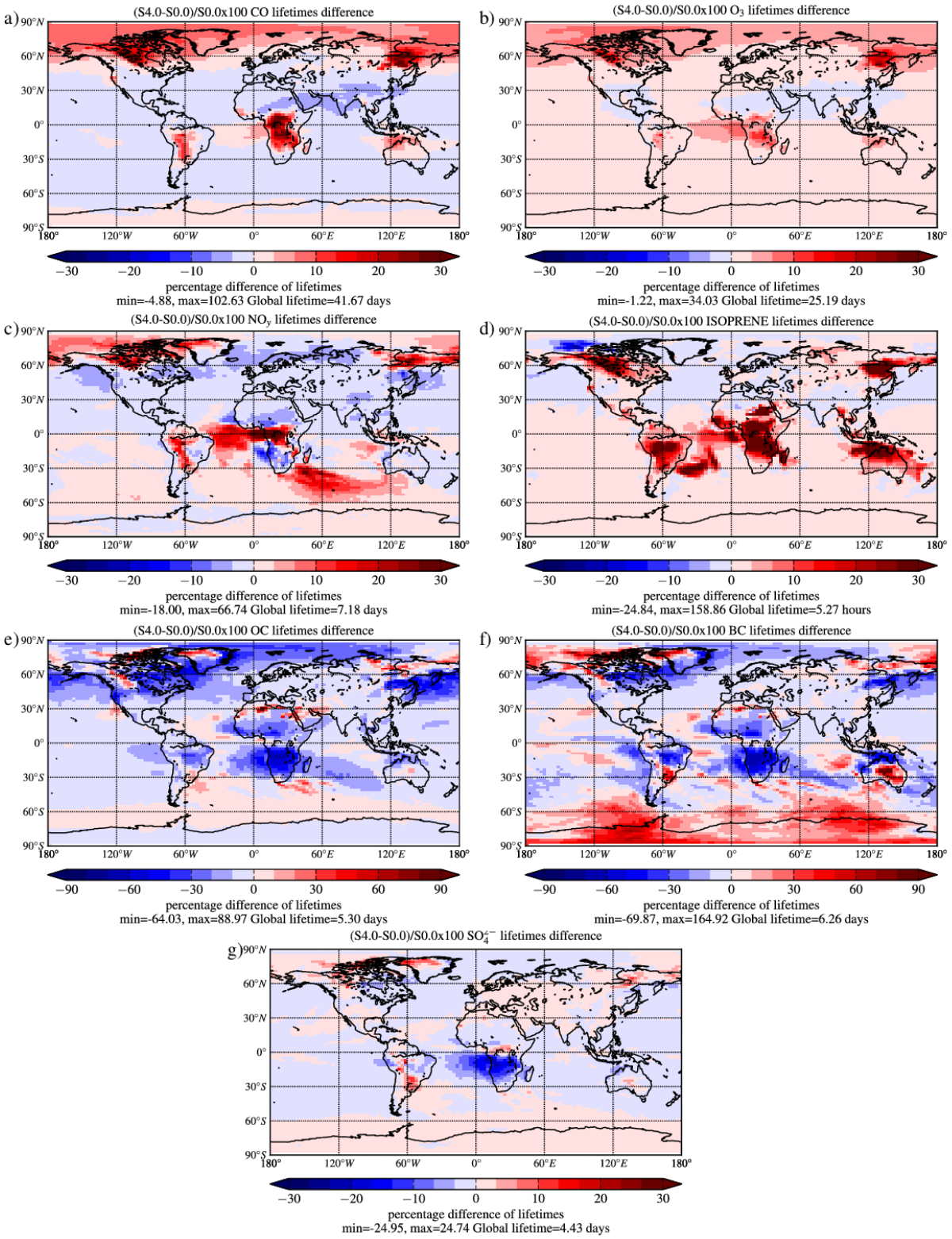

Fig. 10 Percent impact of wild fire emissions to the computed annual mean tropospheric lifetimes of CO **(a)**, O_3 **(b)**, NO_y **(c)**, isoprene **(d)**, OC **(e)**, BC **(f)** and SO_4^{2-} **(g)** depicted as the percentage difference of S4.0 and S0.0. The colorbar ranges from -30% to 30% (-90% to 90% for OC and BC). The minimum and maximum local lifetimes percent changes as well as the global lifetime are printed under each panel.

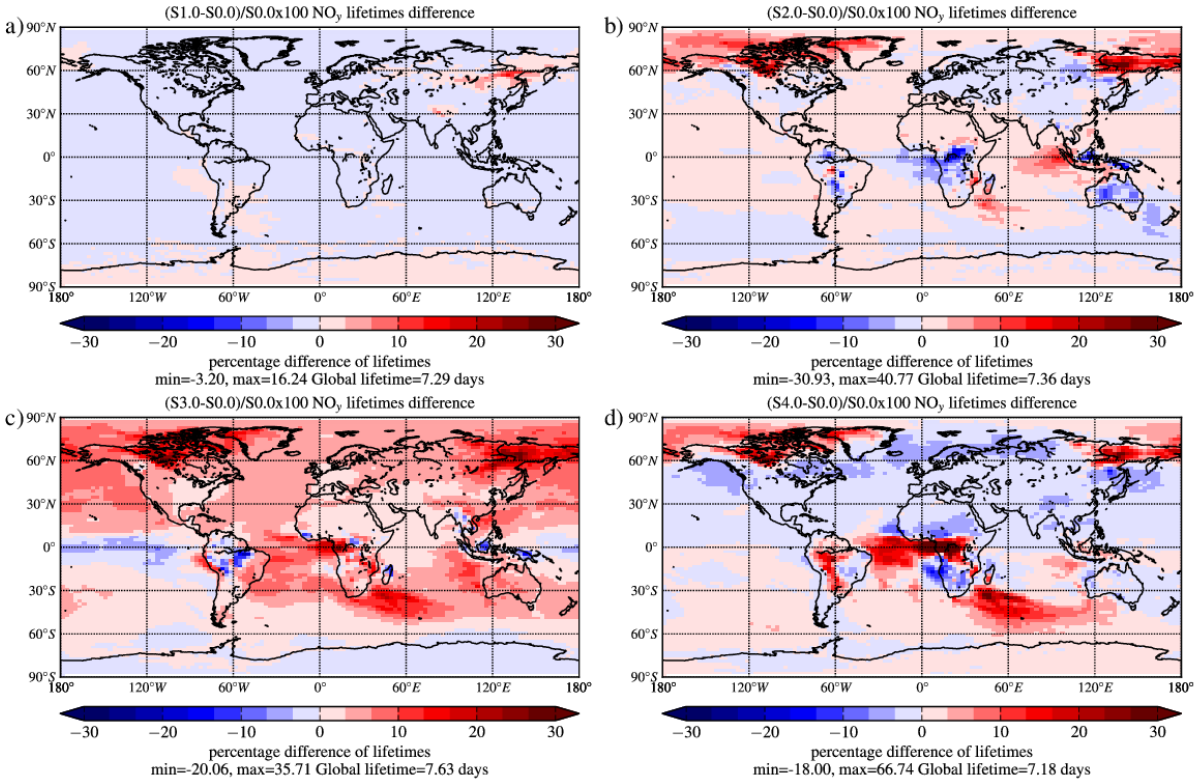

Fig. 11 Computed annual mean tropospheric NO_y lifetimes differences between the base case scenario (S0.0) and S1.0 **(a)**, S2.0 **(b)**, S3.0 **(c)** and S4.0 **(d)**, computed by reference to S0.0. The colorbar ranges from -30% to 30%. The minimum and maximum local lifetimes percent changes as well as the global lifetime are printed under each panel.